Article

Cell Host & Microbe

Secreted *Akkermansia muciniphila* threonyl-tRNA synthetase functions to monitor and modulate immune homeostasis

Graphical abstract

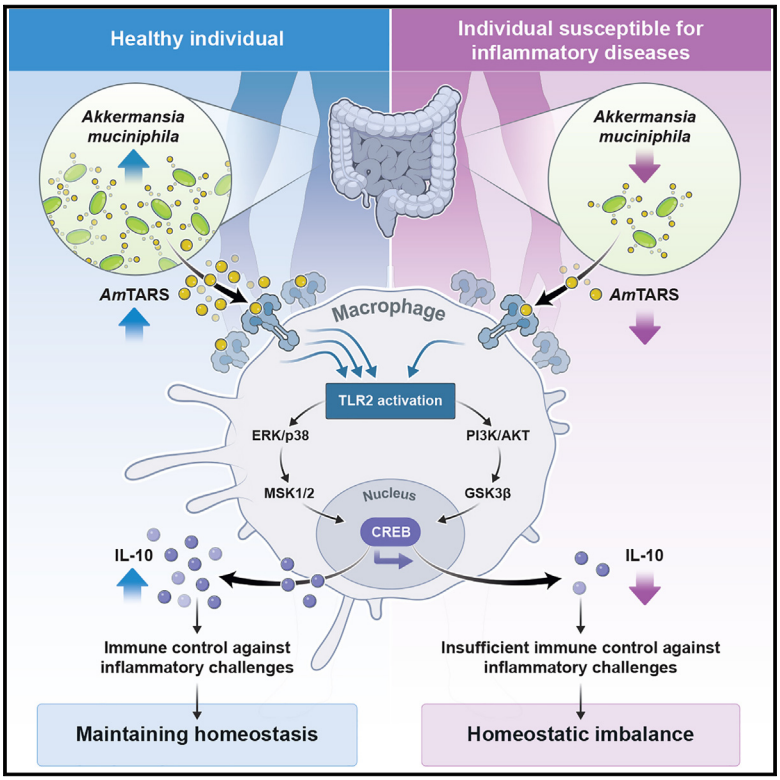

Highlights

- Gut-associated *Akkermansia muciniphila* secretes threonyl-tRNA synthetase (*Am*TARS)
- Secreted *Am*TARS targets macrophages and activates the anti-inflammatory TLR2-CREB axis
- An evolutionarily acquired region in *Am*TARS mediates specific interactions with TLR2
- *Am*TARS restores macrophage homeostasis, increases IL-10, and attenuates colitis in mice

Authors

Su-Man Kim, Shinhye Park, Seung-Ho Hwang, ..., Sunghoon Kim, Won-Jae Lee, Myung Hee Kim

Correspondence

mhk8n@kribb.re.kr

In brief

Kim et al. report that the gut-associated bacterium *A. muciniphila* secretes threonyl-tRNA synthetase (*Am*TARS) to monitor and modulate host immune homeostasis. Secreted *Am*TARS activates anti-inflammatory signaling, restores macrophage homeostasis, increases IL-10, and attenuates colitis in mice. Commensal tRNA synthetases may act as intrinsic mediators that maintain homeostasis.

Kim et al., 2023, Cell Host & Microbe *31*, 1021–1037
June 14, 2023
https://doi.org/10.1016/j.chom.2023.05.007

CellPress

Cell Host & Microbe

CellPress
OPEN ACCESS

Article

Secreted *Akkermansia muciniphila* threonyl-tRNA synthetase functions to monitor and modulate immune homeostasis

Su-Man Kim,[1,2,18] Shinhye Park,[1,3,18] Seung-Ho Hwang,[1] Eun-Young Lee,[1] Jong-Hwan Kim,[4] Ga Seul Lee,[5,6] Giljae Lee,[7] Dong-Ho Chang,[1] Jae-Geun Lee,[1] Jungwon Hwang,[1] Youngjin Lee,[1] Minsoo Kyung,[8] Eun-Kyoung Kim,[8] Jae-Hoon Kim,[9,19] Tae-Hwan Kim,[1,10] Jeong Hee Moon,[5] Byoung-Chan Kim,[1,11] GwangPyo Ko,[7,12,13,14] Seon-Young Kim,[4,15] Ji-Hwan Ryu,[16] Jeong-Soo Lee,[1,15] Chul-Ho Lee,[9,15] Jeong-Yoon Kim,[3] Sunghoon Kim,[17] Won-Jae Lee,[8] and Myung Hee Kim[1,20,*]

[1]Microbiome Convergence Research Center, Korea Research Institute of Bioscience and Biotechnology (KRIBB), Daejeon 34141, Korea
[2]Department of Biology Education, Chonnam National University, Gwangju 61186, Korea
[3]Department of Microbiology and Molecular Biology, Chungnam National University, Daejeon 34134, Korea
[4]Korean Bioinformation Center, KRIBB, Daejeon 34141, Korea
[5]Core Research Facility & Analysis Center, KRIBB, Daejeon 34141, Korea
[6]College of Pharmacy, Chungbuk National University, Cheongju 28160, Chungbuk, Korea
[7]Department of Environmental Health Sciences, Graduate School of Public Health, Seoul National University, Seoul 08826, Korea
[8]National Creative Research Initiative Center for Hologenomics and School of Biological Sciences, Seoul National University, Seoul 08826, Korea
[9]Laboratory Animal Resource Center, KRIBB, Daejeon 34141, Korea
[10]College of Veterinary Medicine, Chungnam National University, Daejeon 34134, Korea
[11]HealthBiome, Inc., Bioventure Center, Daejeon 34141, Korea
[12]Center for Human and Environmental Microbiome, Institute of Health and Environment, Seoul National University, Seoul 08826, Korea
[13]KoBioLabs, Inc., Seoul 08826, Korea
[14]Bio-MAX/N-Bio, Seoul National University, Seoul 08826, Korea
[15]Department of Functional Genomics, KRIBB School of Bioscience, Korea University of Science and Technology, Daejeon 34113, Korea
[16]Severance Biomedical Science Institute and Brain Korea 21 PLUS Project for Medical Science, Yonsei University College of Medicine, Seoul 03722, Korea
[17]Institute for Artificial Intelligence and Biomedical Research, College of Pharmacy and College of Medicine, Gangnam Severance Hospital, Yonsei University, Incheon 21983, Republic of Korea
[18]These authors contributed equally
[19]Present address: Livestock Products Analysis Division, Division of Animal Health, Daejeon Metropolitan City Institute of Health and Environment, Daejeon 34146, Korea
[20]Lead contact
*Correspondence: mhk8n@kribb.re.kr
https://doi.org/10.1016/j.chom.2023.05.007

SUMMARY

Commensal bacteria are critically involved in the establishment of tolerance against inflammatory challenges, the molecular mechanisms of which are just being uncovered. All kingdoms of life produce aminoacyl-tRNA synthetases (ARSs). Thus far, the non-translational roles of ARSs have largely been reported in eukaryotes. Here, we report that the threonyl-tRNA synthetase (*Am*TARS) of the gut-associated bacterium *Akkermansia muciniphila* is secreted and functions to monitor and modulate immune homeostasis. Secreted *Am*TARS triggers M2 macrophage polarization and orchestrates the production of anti-inflammatory IL-10 via its unique, evolutionary-acquired regions, which mediates specific interactions with TLR2. This interaction activates the MAPK and PI3K/AKT signaling pathways, which converge on CREB, leading to an efficient production of IL-10 and suppression of the central inflammatory mediator NF-κB. *Am*TARS restores IL-10-positive macrophages, increases IL-10 levels in the serum, and attenuates the pathological effects in colitis mice. Thus, commensal tRNA synthetases can act as intrinsic mediators that maintain homeostasis.

INTRODUCTION

Co-evolution of the host and its gut microbiota has led to a highly mutualistic relationship in which the gut microbiota plays fundamental roles in maintaining host homeostasis.[1–4] Growing evidence shows that perturbation of the gut microbiota (i.e., dysbiosis) has a marked effect on metabolic and immune processes, eventually affecting host physiology linked to multiple metabolic and inflammatory disorders.[5–7]

Although the association between the gut microbiota and human health and disease, particularly via shaping of the immune system, has become evident, the molecular determinants that

regulate and tune immune homeostasis, and their underlying mechanisms, are still largely unknown. Recent comprehensive studies on commensal bacteria-derived molecules that regulate host immunity have focused on diet-induced metabolites such as short-chain fatty acids and indole derivatives, which act as signaling molecules and maintain immune homeostasis via host receptors and other target molecules.[8–11] Little is known about whether or how the biological systems of commensals are linked to host immunity and physiology.

All kingdoms of life produce enzymes known as aminoacyl-tRNA synthetases (ARSs), which attach appropriate amino acids to cognate tRNAs.[12] Charged tRNAs transfer their amino acids to growing peptide chains in the ribosome during protein synthesis; thus, ARSs are essential for decoding genetic information. However, evidence accumulated over the past few decades suggests that these enzymes have biological roles beyond translation.[13–16] Eukaryotic cytoplasmic ARSs have additional domains and motifs that correlate with functional versatility and system complexity.[13–17] In particular, mammalian ARSs such as tryptophanyl-tRNA synthetase 1 (WARS1 [eukaryotic ARSs are abbreviated using the single-letter code for their corresponding amino acid followed by "ARS1" for cytoplasmic enzymes and by "ARS2" for their mitochondrial counterparts]) are secreted and appear to play roles in physiological activities such as immune regulation, although the mechanism underlying their secretion still remains elusive.[18–21] Due to their multifaceted roles, ARSs are considered mediators that maintain homeostasis by tuning translation, as well as other biological roles.[13,15–17] So far, studies of the non-translational roles of ARSs have focused largely on eukaryotes. To date, little attention has been paid to the role of ARSs of commensals in regulating host homeostasis.

We hypothesized that gut commensal ARSs may contribute to the maintenance of host homeostasis via immune regulation. *A. muciniphila* is the only known species of the *Verrucomicrobia* phylum that stably colonizes the human gut within 1 year after birth.[22] Numerous studies show a correlation between the lack, or decreased abundance, of *A. muciniphila* and multiple diseases[23]; thus, the bacterium has attracted growing interest due to its health-promoting benefits in those with disrupted metabolism and immunity associated with inflammation and metabolic disorders.[24–30] Thus, in this study, we set out to examine the homeostatic roles played by ARSs produced by this organism. We found that *A. muciniphila* secretes threonyl-tRNA synthetase (referred to hereafter as *Am*TARS) under normal steady-state conditions and that secreted *Am*TARS acts as an immune homeostatic mediator by activating the Toll-like receptor 2 (TLR2)-cAMP response element-binding protein (CREB) anti-inflammatory immune axis. Taken together, our results suggest that commensal ARSs may have co-evolved as intrinsic immune mediators, shedding new light on the evolution of host/gut microbiota interactions.

RESULTS

A. muciniphila secretes *Am*TARS to promote anti-inflammatory immune responses

To examine the involvement of commensal ARSs in immune regulation, we purified *A. muciniphila* ARSs (*Am*ARSs) and tested their anti-inflammatory activity against bone marrow-derived macrophages (BMDMs). We found that *Am*TARS, but not other *Am*ARSs, triggered a significant increase in the production of anti-inflammatory IL-10 by BMDMs under steady-state conditions (Figure 1A). In addition, BMDMs treated with TARSs from other representative gut commensals, including *Bacteroides fragilis*, *Escherichia coli*, and *Ruminococcus bromii*, as well as from humans, did not produce IL-10, suggesting a specific role for *Am*TARS in immune regulation (Figure 1B). Next, we asked whether *Am*TARS is secreted extracellularly to play a role in immune regulation. An immunoassay using an *Am*ARS-specific antibody revealed that *A. muciniphila* secretes *Am*TARS, but not tyrosyl-tRNA synthetase (*Am*YARS was used as a control), under normal steady-state conditions (Figure 1C). Communication between Gram-negative bacteria is often mediated through the secretion of soluble mediators and extracellular vesicles (EVs),[31] and the same is true for *A. muciniphila*.[32] Thus, we examined *Am*TARS and detected predominantly in soluble fractions rather than that in EVs purified from culture supernatants (Figures 1D and S1A–S1C).

Of note, although *Am*TARS induced the production of anti-inflammatory IL-10 by BMDMs under normal conditions, it had no effect on the production of pro-inflammatory cytokines IL-6 and TNF-α (Figures 1E–1G). Moreover, *Am*TARS increased IL-10 levels, and suppressed IL-6 and TNF-α, to an even greater extent following the stimulation of BMDMs with lipopolysaccharide (LPS) (Figures 1H–1J). Similar results were observed in *Am*TARS-treated THP1 cells under both normal and inflammatory (LPS) conditions (Figures S1D–S1I). Taken together, these results suggest that the commensal bacterium *A. muciniphila* secretes *Am*TARS to maintain (under normal conditions) and induce (under inflammatory conditions) host immune homeostasis.

*Am*TARS plays an anti-inflammatory role by activating IL-10-positive macrophage polarization

Inflammatory bowel disease (IBD), a chronic disease of the gastrointestinal tract, arises from the complex interplay between genetic, microbial, and environmental factors, leading to aberrant immunological responses and inflammation.[33–35] A recent meta-analysis using the Inflammatory Bowel Diseases Multiomics Database (IBDMDB) within the integrated Human Microbiome Project (iHMP) provided longitudinal multi-omics datasets from IBD patients and non-IBD controls. It provides a comprehensive overview of the gut microbial ecosystem in IBD and identifies a distinctive increase in facultative anaerobes at the expense of obligate anaerobes during active disease.[36] Since several studies demonstrate an inverse correlation between the abundance of the strictly anaerobic commensal bacterium *A. muciniphila* and inflammation and metabolic disorders, including IBD,[37–40] we utilized the IBDMDB to re-evaluate the correlation between the abundance of *A. muciniphila* and IBD. Consistent with previous reports, IBDMDB metagenomic analysis revealed that compared with non-IBD controls, the abundance of *A. muciniphila* is significantly lower in subjects with ulcerative colitis (UC) or Crohn's disease (CD) (Figure S2A). Further functional profiling revealed that the abundance of total bacterial TARS is not significantly lower in subjects with IBD (Figure S2B). However, stratification by individual species revealed that levels of *Am*TARS are significantly lower in those with UC or CD than in non-IBD controls (Figure S2C). The levels of other *Am*ARSs were

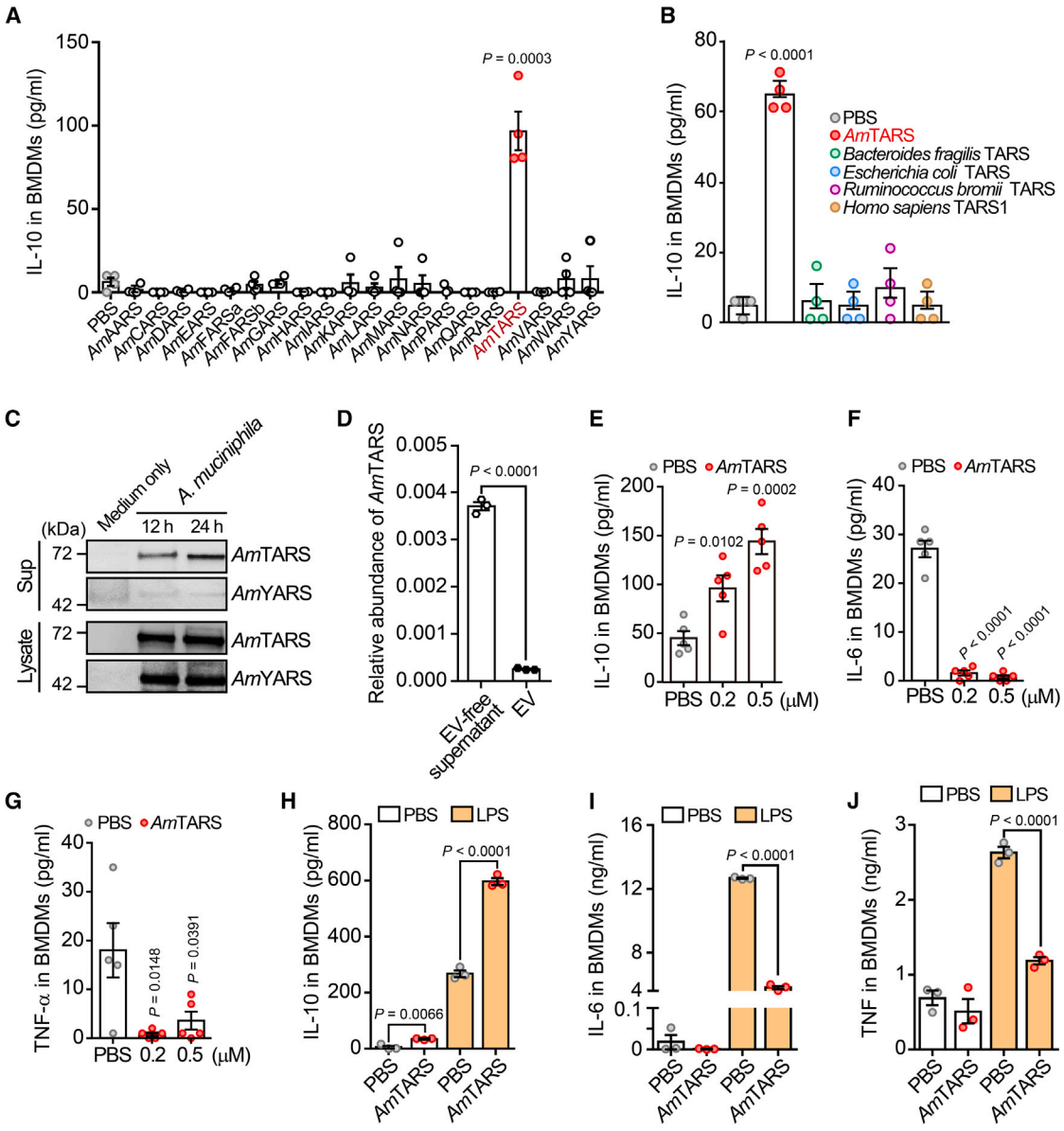

Figure 1. *A. muciniphila* extracellularly secretes *Am*TARS to exert anti-inflammatory immune regulation

(A and B) IL-10 in BMDM culture supernatants treated with 0.5 μM purified *A. muciniphila* aminoacyl-tRNA synthetases (*Am*ARSs) (n = 4 per group) (A) or 0.5 μM purified threonyl-tRNA synthetases (TARSs) of indicated species (n = 4 per group) (B).

(C) Western blot analysis of *Am*TARS secreted into the culture supernatant of *A. muciniphila* under normal conditions. *Am*YARS was analyzed as a control.

(D) Relative abundance of *Am*TARS in soluble fractions and in EVs purified from culture supernatants (n = 3 per group).

(E–J) Levels of IL-10, IL-6, and TNF-α in BMDMs treated with 0.5 μM *Am*TARS under normal conditions (n = 5 per group) (E–G) or with 0.5 μM *Am*TARS under LPS (10 ng mL^{-1})-induced inflammatory conditions for 24 h (n = 3 per group) (H–J).

PBS, phosphate-buffered saline; *Am*AARS, alanyl-tRNA synthetase; *Am*CARS, cysteinyl-tRNA synthetase; *Am*DARS, aspartyl-tRNA synthetase; *Am*EARS, glutamyl-tRNA synthetase; *Am*FARSa, phenylalanyl-tRNA synthetase alpha subunit; *Am*FARSb, phenylalanyl-tRNA synthetase beta subunit; *Am*GARS, glycyl-tRNA synthetase; *Am*HARS, histidyl-tRNA synthetase; *Am*IARS, isoleucyl-tRNA synthetase; *Am*KARS, lysyl-tRNA synthetase; *Am*LARS, leucyl-tRNA synthetase; *Am*MARS, methionyl-tRNA synthetase; *Am*NARS, asparaginyl-tRNA synthetase; *Am*PARS, prolyl-tRNA synthetase; *Am*QARS, glutaminyl-tRNA synthetase; *Am*RARS, arginyl-tRNA synthetase; *Am*TARS, threonyl-tRNA synthetase; *Am*VARS, valyl-tRNA synthetase; *Am*WARS, tryptophanyl-tRNA synthetase; *Am*YARS, tyrosyl-tRNA synthetase; EV, extracellular vesicle.

Data shown in (A), (B), and (D)–(J) are representative of at least three independent experiments, each with similar results (mean ± SEM). p values were calculated using an unpaired two-tailed Student's t test. Data shown in (C) are representative of three independent experiments.

also lower in subjects with UC or CD (Figure S2D), suggesting that the levels of *Am*ARSs correlate with the abundance of *A. muciniphila*. Further metatranscriptomic analysis also showed that there was no difference between the abundance of TARS from all bacteria in those with or without IBD but also that *Am*TARS levels in UC subjects were significantly lower than those in non-IBD subjects (Figures S2E and S2F). Expression levels of TARS from the top ten contributors were not significantly different between IBD subjects and non-IBD subjects (Figure S2G). Consistent with the metagenomics results, we found that the expression of other *Am*ARSs was lower in IBD subjects than that in non-IBD subjects (Figure S2H). Overall, these data suggest that a reduced abundance of *A. muciniphila* is associated with lower levels of *Am*TARS, leading to the dysregulation of *Am*TARS-mediated anti-inflammatory immune responses in patients with IBD.

To validate this hypothesis, we evaluated the anti-inflammatory function of *Am*TARS in a mouse model of dextran sulfate sodium (DSS)-induced colitis. First, we evaluated the stability of intraperitoneal (i.p.)-administered *Am*TARS *in vivo*. *Am*TARS was observed for 3 days post-administration (Figures S3A and S3B). Subsequently, we assessed dose-dependent responses (i.e., changes in body weight and colon length) after i.p. administration of *Am*TARS (0.05–0.4 mg kg^{-1}) once every other day for 10 days (Figure 2A). Overall, administration of *Am*TARS attenuated body weight loss and colon shortening in a dose-dependent manner (up to 0.2 mg kg^{-1}) (Figures S3C and S3D). Administration of *Am*TARS at a dose of 0.4 mg kg^{-1} significantly attenuated body weight loss for up to 7 days but yielded similar outcomes to those in colitis mice treated with phosphate-buffered saline (PBS) by day 10, suggesting that high doses of *Am*TARS may have adverse effects (Figures S3C and S3D). Thus, we used a dose of 0.2 mg kg^{-1} for further *in vivo* evaluation of the anti-inflammatory immune effects of *Am*TARS. i.p. administration of *Am*TARS ameliorated disease activity scores, in addition to body weight loss and colon shortening, in colitis mice (Figures 2B, S3E, and S3F). Disruption of the epithelial lining and the damage score, particularly in the proximal colon, were significantly lower in *Am*TARS-treated colitis mice than in control mice (Figures 2C and 2D).

To identify the cells targeted by *Am*TARS, mice were i.p.-injected with fluorescently labeled *Am*TARS, and fluorescence-positive cells in peritoneal exudate cells (PECs) were analyzed by flow cytometry. Fluorescently labeled Alexa568-*Am*TARS was detected predominantly on macrophages ($F4/80^+$) rather than T cells ($CD3^+$) and B cells ($CD19^+$) (Figure 2E). Next, we used a Mac2 immunofluorescent antibody to test whether i.p.-injected *Am*TARS targets intestinal macrophages. First, we validated whether the anti-6X His tag antibody interacted specifically with administered His-tagged *Am*TARS (detected using an anti-*Am*TARS antibody). There was clear co-localization of the His tag with *Am*TARS, indicating that anti-6X His tag antibody specifically detects administered *Am*TARS (Figure S3G). Strong expression of Mac2 was detected in the colonic epithelium, as well as in macrophages located in the lamina propria. Administered *Am*TARS co-localized mainly with macrophages in the lamina propria, demonstrating that *Am*TARS targets macrophages in the gut (Figure 2F). We also questioned whether systemically administered *Am*TARS acts directly on residential F4/80-positive macrophages or on the cells migrated from the systemically stimulated peritoneal macrophage population. To address this, we carried out adoptive transfer experiments using CD45.1 and CD45.2 mice as recipients and donors, respectively. PECs, including macrophages ($F4/80^+CD45.2^+$), from CD45.2 mice were transferred intraperitoneally into CD45.1 mice. Macrophages from the transferred PECs population were observed in the peritoneal cavity of CD45.1 mice administered PBS or AmTARS at days 5 and 10, respectively. However, no transferred macrophages were detected in the colon of CD45.1 mice (Figure S3H). These data suggest that systemically administered *Am*TARS seems to act directly on residential macrophages. We isolated macrophages from the peritoneal cavity and intestine and further validated *Am*TARS-mediated production of anti-inflammatory IL-10 (Figures 2G, 2H, S3I and S3J).

Since M2 macrophage polarization precedes the production of anti-inflammatory cytokines such as IL-10, we assessed the effects of *Am*TARS on macrophage polarization. BMDMs were treated with PBS (negative control), LPS (10 ng mL^{-1}; to induce inflammation), or IL-4/IL-13 (to induce M2 polarization; positive control) in the absence and presence of *Am*TARS, and the resulting M2 macrophage population was measured by flow cytometry using an antibody specific for the M2 macrophage surface marker CD206. Notably, *Am*TARS activated M2 polarization even in PBS-treated cells and induced significant M2 polarization of cells under LPS-induced inflammatory conditions (Figures 2I and 2J). M2 polarization was fully induced by IL-4/IL-13, as previously reported,[41,42] in both the absence and presence of *Am*TARS (Figures 2I and 2J). Consequently, *Am*TARS significantly suppressed colitis-induced infiltration of inflammatory monocytes ($CD11b^+F4/80^-$), restored IL-10-positive macrophage ($CD11b^+F4/80^+IL\text{-}10^+$) numbers within colonic cells, and increased IL-10 levels in the serum (Figures 2K–2N).

To further validate the macrophage-dependent function of *Am*TARS in improving colitis, we investigated the anti-inflammatory effects of *Am*TARS in macrophage-depleted colitis mice. Consistent with the physiological data, *Am*TARS did not affect the numbers of inflammatory monocytes or IL-10-positive macrophages in macrophage-depleted mice (Figures S4A–S4C). Thus, *Am*TARS had no effect on colitis-induced body weight loss, shortening of the colon, the damage score, the disease activity score, or disruption of the epithelial lining in macrophage-depleted mice (Figures 2O, 2P, and S4D–S4F), further confirming the macrophage-specific functions of *Am*TARS. Collectively, these results indicate that *Am*TARS plays an anti-inflammatory cytokine-like role by activating IL-10-positive macrophage polarization.

*Am*TARS assimilates unique regions to exert immune modulatory functions

To uncover the molecular mechanism underlying the anti-inflammatory immune function of *Am*TARS, we compared its amino acid sequence with that of human TARS1 and with those of TARSs from bacterial species representative of the gut microbiota. *Am*TARS contains two additional unique regions within its N-terminal (residues 99–113, hereafter referred to as U1) and catalytic (residues 290–312, hereafter referred to as U2) domains, which are not found in other TARSs (Figure S4G). In

CellPress
OPEN ACCESS

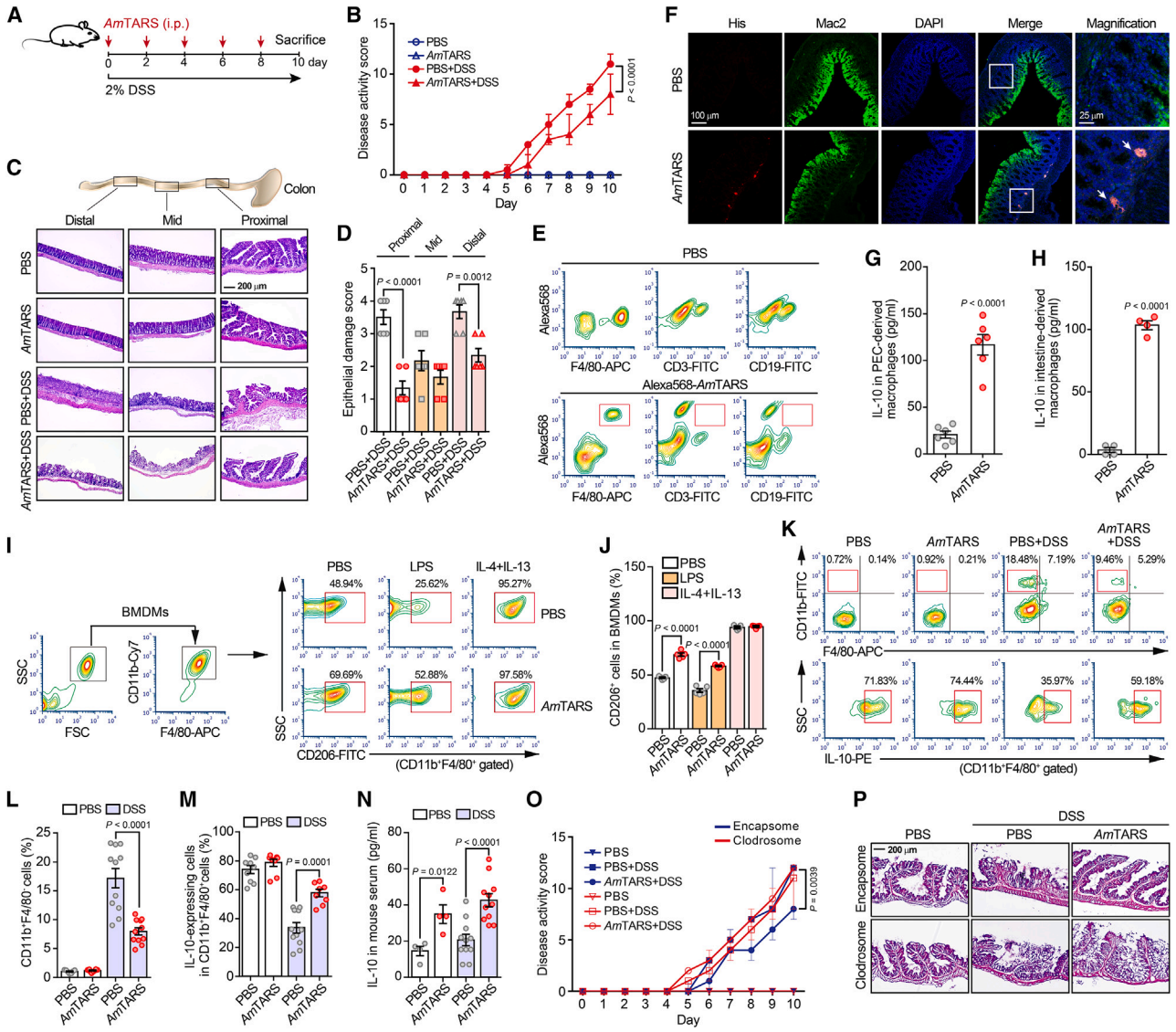

Figure 2. *Am*TARS ameliorates DSS-induced colitis in mice by activating IL-10-positive macrophages

(A–D) Normal or DSS-induced colitis mice injected intraperitoneally (i.p.) with PBS or *Am*TARS. Experimental scheme (A) and daily changes in disease activity scores (n = 10 per group) (B). Representative hematoxylin and eosin staining (H&E) of distal, mid, and proximal regions of the colon (C), and epithelial damage scores (n = 6 per group) (D).

(E) Flow cytometric analysis of the *Am*TARS-targeted cells. Macrophages ($F4/80^+$), B cells ($CD19^+$), and T cells ($CD3^+$) were analyzed in PECs isolated from mice i.p.-injected with PBS or Alexa 568-labeled *Am*TARS (0.5 mg kg^{-1}) for 1 day.

(F) Immunofluorescence staining to detect co-localization of *Am*TARS (His) and macrophages (Mac2) in the colon of mice treated for 1 day with His-tagged *Am*TARS (0.2 mg kg^{-1}).

(G and H) Amount of IL-10 secreted by PEC-derived macrophages (n = 6 per group) (G) and intestine-derived macrophages (n = 4 per group) (H) from mice treated with PBS or 0.5 μM *Am*TARS.

(I) Flow cytometry analysis of $CD206^+$ cells within BMDMs treated for 24 h with PBS, LPS (10 ng mL^{-1}), or IL-4 (20 ng mL^{-1}) + IL-13 (20 ng mL^{-1}).

(J) Percentage of $CD206^+$ cells in (I) (n = 5 per group).

(K–N) Normal or DSS-induced colitis mice were treated with PBS or *Am*TARS. Representative flow cytometry plots showing monocytes (upper panel, $CD11b^+$), macrophages ($CD11b^+F4/80^+$), and IL-10-positive macrophages (lower panel) within colon cells (K). Percentage of $CD11b^+F4/80^-$ (n = 7, 8, 11, and 11 per group) (L) and IL-10-expressing macrophages (n = 9, 8, 11, and 8 per group) in the mice shown in (M). IL-10 levels in mouse serum (n = 4, 4, 12, and 12 per group) (N).

(O and P) Macrophage-dependent *Am*TARS function (n = 5 per group). Daily disease activity score (O) and H&E staining in the proximal colon (P) of DSS-induced colitis mice in which macrophages were depleted by Clodrosome treatment. Encapsome treatment was included as a Clodrosome control.

Data shown in (B), (D), (G), (H), (J), and (L)–(O) are representative of three independent experiments, each with similar results (mean ± SEM). p values were calculated by an unpaired two-tailed Student's t test. Data shown in (C), (E), (F), and (P) are representative of three independent experiments.

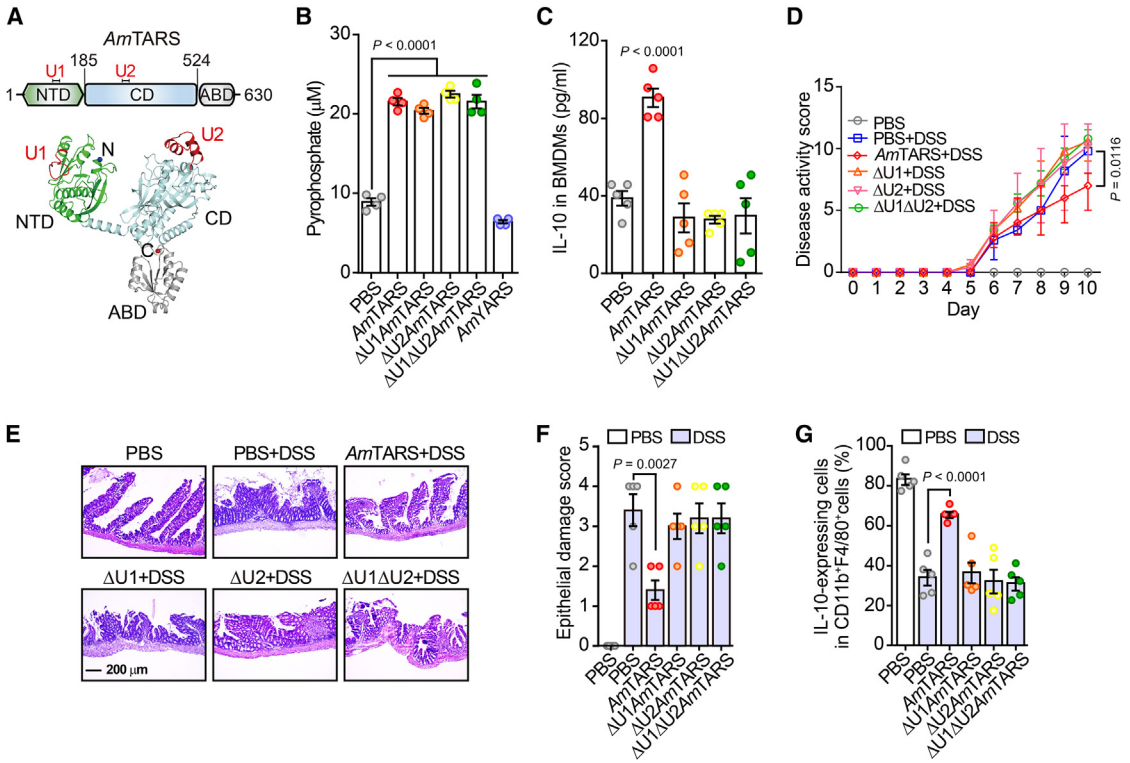

Figure 3. Unique regions in *Am*TARS are essential for anti-inflammatory immune regulation

(A) A structural model of *Am*TARS based on the crystal structure of *S. aureus* TARS (PDB: 1NYQ). The unique regions (U1 and U2) in *Am*TARS are indicated in red.

(B) Amino-acylation activity assay of *Am*TARS and its unique region-deleted mutants. (ΔU1*Am*TARS, ΔU2*Am*TARS, and ΔU1ΔU2*Am*TARS) (n = 4 per group). *Am*YARS was used as a negative control.

(C) IL-10 production by BMDMs treated with *Am*TARS or unique region-deleted *Am*TARS mutants (n = 5 per group).

(D–G) DSS-induced colitis mice treated with *Am*TARS or unique region-deleted *Am*TARS mutants (n = 5 per group). Daily changes in the disease activity score (D). H&E staining of the proximal colon (E). Scoring of epithelial damage in (F). Percentage of $CD11b^{+}F4/80^{+}IL\text{-}10^{+}$ cells within colon cells (G).

Data shown in (B)–(D), (F), and (G) are representative of three independent experiments, each with similar results (mean ± SEM). p values were calculated by an unpaired two-tailed Student's t test. Data shown in (E) are representative of three independent experiments.

addition, Blast-based sequence searches (https://blast.ncbi.nlm.nih.gov/Blast.cgi) detected no sequences with significant homology to the unique regions, suggesting that these unique regions may have been evolutionarily assimilated by *A. muciniphila* specifically for immune regulation.

Next, we modeled the structure of *Am*TARS using AlphaFold[43] and found that it showed significant structural similarity to other TARSs, including *Staphylococcus aureus* TARS (PDB: 1NYQ) and human TARS1 (PDB: 4HWT), except for the unique regions (Figures S4H and S4I). The structural model suggests that both U1 and U2 within *Am*TARS are surface-exposed and may be involved in the interaction with host targets such as signaling receptors (Figure 3A). Subsequently, we evaluated the functionality of U1 and U2 by generating mutant proteins (ΔU1, ΔU2, and ΔU1ΔU2) harboring deletions in these unique regions. Neither mutant protein was different from the wild-type (WT) *Am*TARS with respect to its enzymatic activity (Figure 3B) but abolished the IL-10 production in BMDMs (Figure 3C). Consequently, neither mutant protein promoted recovery of body weight loss, disease activity scores, shortening of the colon, or epithelial lining disruption and damage scores, in colitis-induced mice (Figures 3D–3F, S4J, and S4K). The positive immune regulatory functions of *Am*TARS that reduced colitis-induced pro-inflammatory monocytes and enhanced IL-10-positive macrophages in the colon were eliminated when mutant *Am*TARSs were administered to colitis mice (Figures 3G and S4L). Similar to WT *Am*TARS, the ΔU1ΔU2 mutant had no effect on colitis-induced body weight loss, disease activity score, or shortening of the colon in macrophage-depleted mice (Figures S4M–S4O). Thus, these data clearly demonstrate that the unique regions U1 and U2 within *Am*TARS are essential for their anti-inflammatory function.

*Am*TARS is a TLR2 ligand that activates anti-inflammatory immune responses

To identify the host target of *Am*TARS, we performed membrane protein interactome analysis using THP1 cells. Several potential interactors, which are receptors involved in innate immunity, were identified (Figure S5A), and their interactions with *Am*TARS were evaluated using a pull-down assay. The results suggested that among the candidates tested, *Am*TARS interacted only with TLR2 (Figures 4A, S5B, and S5C); thus, TLR2 may be the receptor targeted by *Am*TARS to trigger IL-10-mediated anti-inflammatory immune regulation. By contrast, the pull-down assay clearly

CellPress
OPEN ACCESS

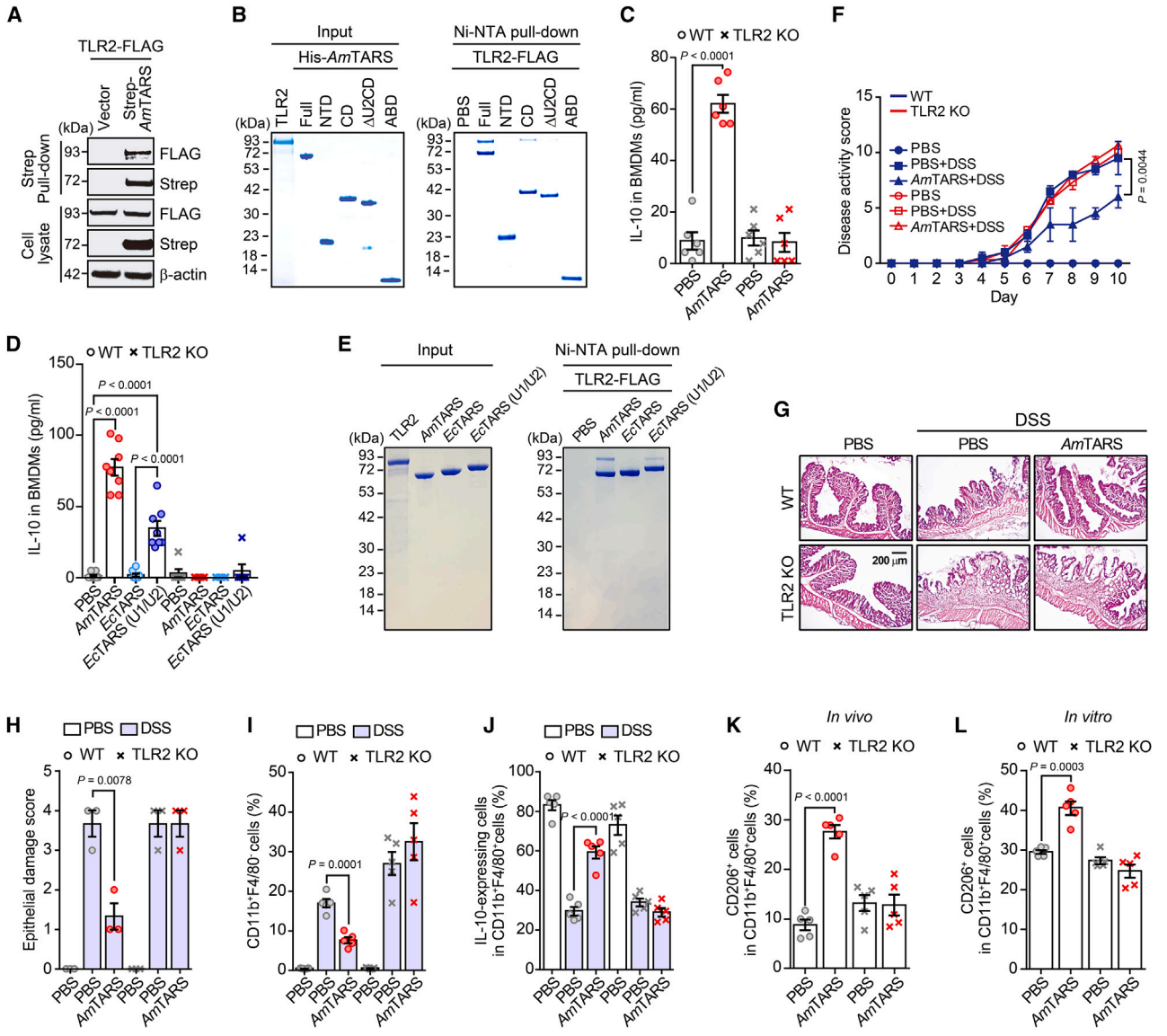

Figure 4. *Am*TARS is a TLR2-dependent anti-inflammatory immune mediator

(A and B) *Am*TARS interacts directly with TLR2. Pull-down assay using lysates of HEK 293T cells transfected with Strep-*Am*TARS and TLR2-FLAG (A). The proteins precipitated by an anti-Strep antibody were analyzed by western blotting. *In vitro* interaction assay using purified TLR2-FLAG and His-tagged *Am*TARS proteins (B). Purified TLR2-FLAG was mixed with purified His-tagged *Am*TARS protein. His-tagged protein was precipitated by Ni-NTA, eluted, and analyzed by SDS-PAGE.

(C) TLR2-dependent anti-inflammatory function of *Am*TARS in BMDMs (n = 6 per group).

(D) The unique regions within *Am*TARS are essential for anti-inflammatory function in a TLR2-dependent manner (n = 8 per WT group and n = 6 per TLR2 KO group). BMDMs from WT or TLR2-KO mice were treated with the indicated proteins (C and D).

(E) U1/U2 region-dependent interaction with TLR2. Purified TLR2-FLAG was mixed with purified His-tagged *Am*TARS, *Ec*TARS, and *Ec*TARS (U1/U2) protein. His-tagged proteins were then precipitated by an Ni-NTA resin and analyzed by SDS-PAGE.

(F–J) TLR2-dependent function of *Am*TARS *in vivo*. WT or TLR2-KO mice with DSS-induced colitis were injected with either PBS or *Am*TARS. Daily changes in disease activity scores (n = 10 per group) (F). Intestinal epithelial damage, as analyzed by H&E staining (G), and damage scores (n = 3 per group) (H). Percentage of infiltrated immune cells, gated on $CD11b^+F4/80^-$ (monocytes) (I) and $CD11b^+F4/80^+IL\text{-}10^+$ (IL-10-secreting macrophages) (n = 5 per group) (J).

(K and L) TLR2-dependent M2 macrophage polarization induced by *Am*TARS. WT or TLR2-KO mice were i.p. injected with either PBS or *Am*TARS (n = 5 per group) (K). After 24 h, PECs were isolated, and the percentage of M2 macrophages ($CD206^+$ $CD11b^+F4/80^+$) was measured by flow cytometry. Percentage of M2 macrophages in BMDMs from WT or TLR2-KO mice treated for 24 h with either *Am*TARS or PBS (n = 5 per group) (L).

*Ec*TARS, *E. coli* TARS; *Ec*TARS (U1/U2), an engineered *Ec*TARS incorporating the *Am*TARS U1 and U2 regions. Data shown in (A), (B), (E), and (G) are representative of three independent experiments. Data shown in (C), (D), (F), and (H)–(L) are representative of three independent experiments, each with similar results (mean ± SEM). p values were calculated by an unpaired two-tailed Student's t test.

showed no interaction between *Am*TARS and TLR4 (Figure S5D). To further validate the interaction between *Am*TARS and TLR2, *in vitro* pull-down assays were performed using purified TLR2 and *Am*TARS proteins (Figure 4B). The results clearly showed that *Am*TARS interacts directly with TLR2 via the U2-containing catalytic domain (CD). The interaction between the U2-deleted CD (ΔU2CD) protein and TLR2 was markedly weaker. There was no direct interaction between the U1-containing N-terminal domain (NTD) and TLR2. TLR2 functions by forming either a homodimer or a heterodimer with TLR1 or TLR6.[44] Thus, U1 might be involved in the interaction with the heterodimers.

The TLR2-dependent immune function of *Am*TARS was further corroborated using TLR2 knockout (KO) mice. *Am*TARS did not induce IL-10 production in BMDMs from TLR2-KO mice, demonstrating that the interaction between *Am*TARS and TLR2 is indispensable for anti-inflammatory immune activation (Figure 4C). We furthermore confirmed the requirement of the unique regions for the TLR2-dependent immune function of *Am*TARS by engineering *E. coli* TARS (*Ec*TARS), which had no anti-inflammatory immune function in BMDMs (Figure 1B). Incorporation of the *Am*TARS U1 and U2 sequences into the corresponding regions in *Ec*TARS (*Ec*TARS (U1/U2)) conferred the ability to trigger IL-10 production on *Ec*TARS via the interaction with TLR2 (Figures 4D and 4E). However, IL-10 production by *Ec*TARS (U1/U2) was abolished in BMDMs from TLR2-KO mice, providing further evidence that *Am*TARS regulates host immune cells via its unique regions in a TLR2-dependent manner (Figure 4D). We furthermore confirmed the functionality of the unique regions *in vivo* using *Ec*TARS (U1/U2). DSS-induced colitis mice were i.p.-injected with *Ec*TARS (U1/U2) at a dose of 0.4 mg kg^{-1} based on its ability to induce IL-10 compared with *Am*TARS in BMDMs (Figure 4D). i.p. administration of *Ec*TARS (U1/U2) ameliorated body weight loss, colon shortening, and epithelial disruption of the colon similar to *Am*TARS administration in colitis mice (Figures S5E–S5G). *Ec*TARS (U1/U2) significantly restored IL-10-positive macrophages in the colon and increased IL-10 levels in the serum (Figures S5H and S5I). Collectively, these data strongly demonstrate that the unique regions U1 and U2 within *Am*TARS are essential prerequisites for its anti-inflammatory immune function.

Subsequently, we assessed the role of TLR2 in *Am*TARS function *in vivo*. TLR2-KO mice were slightly more susceptible to DSS-induced colitis than WT mice, as reported previously.[45] Nevertheless, colitis-induced body weight loss and the disease activity score in TLR2-KO mice did not improve after *Am*TARS treatment (Figures 4F and S5J). The same was true for the shortening of the colon length, disruption of the epithelial lining, and the damage score (Figures 4G, 4H, and S5K). Consistent with these results, *Am*TARS did not induce either a reduction in pro-inflammatory monocyte numbers or an increase in IL-10-secreting macrophage numbers in colitis TLR2-KO mice (Figures 4I and 4J). Furthermore, *Am*TARS did not cause M2 macrophage polarization of peritoneal macrophages from TLR2-KO mice under non-inflammatory conditions (Figure 4K). Likewise, no M2 macrophages were observed in PECs isolated from TLR2-KO mice (Figure 4L). These results strongly suggest that *Am*TARS is a commensal-derived TLR2 ligand required to maintain host immune homeostasis.

*Am*TARS/TLR2 efficiently induces anti-inflammatory responses by activating CREB

Although TLRs play important roles in stimulating inflammation to protect the host from microbial infection, these receptors also regulate anti-inflammatory signaling, which is critical for preventing excessive inflammatory cytokine production and for resolving inflammation.[46,47] TLRs trigger anti-inflammatory signaling via the mitogen-activated protein kinase (MAPK) or phosphoinositide 3-kinases (PI3K)/protein kinase B (AKT) pathways in macrophages,[48] which converge to activate CREB.[49] This transcriptional factor CREB regulates a number of cellular responses, including the production of anti-inflammatory IL-10 by macrophages.[50–52] To identify the signaling pathway triggered by *Am*TARS, we first evaluated kinases and CREB. IL-10 production and M2 polarization were measured in BMDMs treated with inhibitors of extracellular signal-regulated kinase (ERK; PD98059), mitogen-activated protein kinase p38 (p38; SB203580), mitogen- and stress-activated kinase (MSK) 1/2 (SB747651A), CREB (666-15), PI3K (wortmannin), and AKT (AKT1/2) before subsequent stimulation with *Am*TARS. Inhibition of each of these molecules resulted in a significant suppression of IL-10 production (Figure 5A) and macrophage polarization (CD206 positive) by *Am*TARS (Figure 5B), suggesting that *Am*TARS triggers the MAPK and PI3K/AKT signaling pathways to induce anti-inflammatory responses.

Subsequently, we conducted immunoblotting assays to measure the time-dependent activation of *Am*TARS/TLR2-induced signaling molecules in both BMDMs and THP1 cells. *Am*TARS rapidly activated ERK, p38, and MSK1/2 within 15 min and, subsequently, phosphorylation of CREB at Ser133 (which is essential for IL-10 production)[52] within 30 min in BMDMs (Figure 5C) and THP1 cells (Figure 5D). We then compared *Am*TARS-triggered TLR2 signaling with typical ligand-triggered signaling using Pam3CSK4 (the synthetic canonical TLR2/1 agonist, referred to hereafter as Pam3) in BMDMs stimulated for 30 min. Overall, the TLR2-dependent activation pattern of the signaling molecules in the *Am*TARS-triggered pathway was similar to that of molecules triggered by Pam3, which was completely blocked by a TLR2 antibody (Figure 5E). However, significantly greater activation of CREB was observed in *Am*TARS-treated BMDMs than in Pam3-treated BMDMs (Figure 5E). By contrast, activation of NF-κB was greater in Pam3-treated BMDMs than in *Am*TARS-treated BMDMs (Figure 5E). CREB phosphorylated at Ser133 inhibits NF-κB activation by competing for limited amounts of their shared coactivator, CREB-binding protein (CBP)/p300, thereby suppressing pro-inflammatory responses.[49,53,54] Our results show that *Am*TARS induces the production of IL-10 and even inhibits the production of pro-inflammatory cytokines IL-6 and TNF-α in macrophages under inflammatory conditions (Figures 1H–1J and S1G–S1I). These data indicate that, distinct from typical TLR2 ligands, *Am*TARS is a gut commensal-derived TLR2 ligand that maintains immune homeostasis by limiting inflammatory signaling.

*Am*TARS activated PI3K and AKT, and subsequently inhibited GSK3β activity via AKT-mediated phosphorylation at Ser9, in BMDMs (Figure 5F) and THP1 cells (Figure 5G) within 15 min. TLR-stimulated inhibition of GSK3β also increases the association between coactivator CBP and CREB, rather than NF-κB, thereby increasing IL-10 production and suppressing the release of

CellPress
OPEN ACCESS

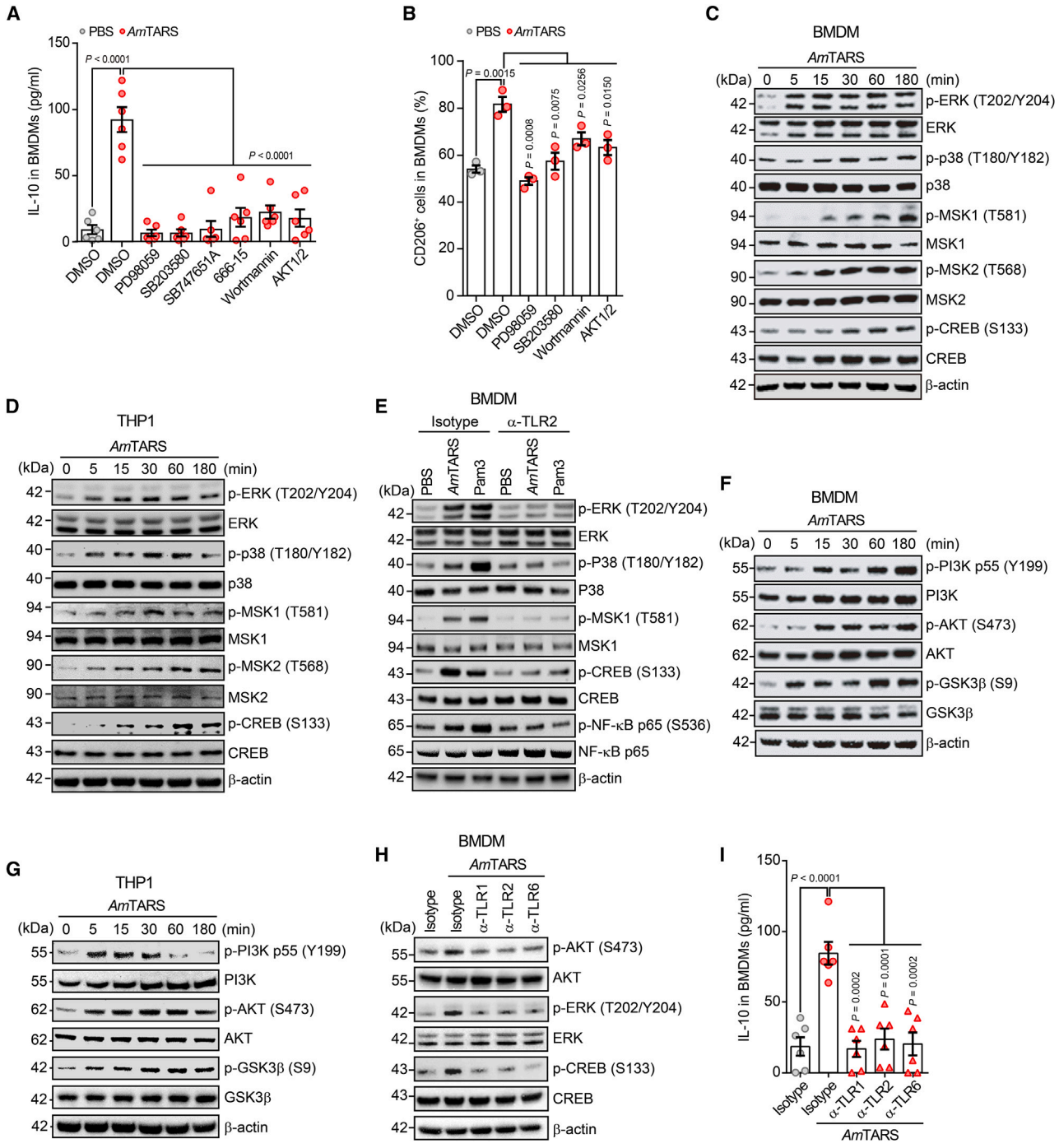

Figure 5. *Am*TARS efficiently promotes anti-inflammatory responses by activating CREB

(A and B) Analysis of key molecules that inhibit the MAPK and PI3K/AKT signaling pathways. IL-10 produced by BMDMs pre-treated with inhibitors of ERK (PD98059, 10 μM), p38 (SB203580, 10 μM), MSK1/2 (SB747651A, 10 μM), CREB (666-15, 1 μM), PI3K (wortmannin, 10 μM), and AKT1/2 (AKT1/2, 10 μM) for 1 h before treatment with either PBS or *Am*TARS for 24 h (n = 6 per group) (A). Flow cytometry analysis of M2 macrophages in BMDMs pre-treated for 1 h with the indicated kinase inhibitors, before treatment with either PBS or *Am*TARS for 24 h (n = 3 per group) (B).

(C and D) Western blot analysis of MAPK signaling molecules in lysates of BMDMs (C) or THP1 cells (D) treated for different times with 0.5 μM *Am*TARS.

(E) Western blot analysis of lysates of BMDMs pre-treated with α-IgG (isotype, 1 μg mL^{-1}) or α-TLR2 (1 μg mL^{-1}) for 1 h before treatment with PBS, *Am*TARS (0.5 μM), or Pam3 (0.5 μM) for 30 min.

(F and G) Western blot analysis of PI3K/AKT signaling molecules in lysates of BMDMs (F) or THP1 cells (G) treated with 0.5 μM *Am*TARS.

(legend continued on next page)

pro-inflammatory cytokines.[55] Thus, these data demonstrate that the interaction between *Am*TARS and TLR2 efficiently activates CREB by triggering the MAPK and PI3K/AKT signaling pathways.

Since TLR2 forms heterodimers with either TLR1 or TLR6 during activation, we assessed which form is targeted by *Am*TARS. An immunoassay showed that *Am*TARS-induced TLR2 signaling is shut down by antibodies targeting TLR1, TLR6, and TLR2, suggesting that *Am*TARS targets both the TLR2/1 and TLR2/6 heterodimers as well as the TLR2 homodimer form to activate anti-inflammatory signaling (Figures 5H and 5I).

We next performed global gene expression profiling of BMDMs treated with *Am*TARS or Pam3 for 1 or 3 h (Figure 6A). Principal-component analysis (PCA) revealed a similar gene expression pattern for *Am*TARS and Pam3 at 1 h, but clearly different profiles at 3 h (Figure 6B). The number of genes whose expression was affected by *Am*TARS, and the extent of their (up- or down-) regulation, was substantially dissimilar to those affected by Pam3, further indicating that *Am*TARS acts as an immune regulator distinct from typical TLR2 ligands (Figure S6A). Subsets of genes showing different expression patterns between *Am*TARS and Pam3 were classified into six clusters by hierarchical clustering analysis (Figures S6A and S6B). The gene expression pattern at 3 h was particularly different for clusters 3 and 4 (Figures 6C, S6A, and S6B). In general, genes belonging to clusters 3 and 4 are associated with inflammation and anti-inflammation, respectively (Figure 6C).

Gene set enrichment analysis revealed a significant induction of inflammatory response-related genes in Pam3-treated BMDMs, consistent with the results from previous reports[51,56] (Figure 6D). However, *Am*TARS-treated cells showed no induction of inflammatory response-related genes (Figure 6D). Notably, the treatment of BMDMs with Pam3 was significantly associated with the upregulation of inflammation-related transcription factors such as NF-κB, RELA, and TFAP2A, whereas *Am*TARS treatment was associated with the upregulation of the anti-inflammation-related transcription factor CREB (Figure 6E). These gene expression profiles correlated positively with the *Am*TARS-TLR2-CREB axis-mediated anti-inflammatory signaling that maintains immune homeostasis via steady-state production of IL-10.

We validated the anti-inflammatory function of *Am*TARS using the *Tg*(*NFκB:EGFP*) zebrafish transgenic line, which allows monitoring of NF-κB activity *in vivo*.[57] Consistent with the gene set enrichment analysis patterns (Figures 6D and 6E) and the signaling pathway results (Figures 5C–5G), the increased NF-κB activity in the distal intestine of zebrafish larvae induced by repeated DSS treatment was significantly dampened by *Am*TARS (Figures 6F–6H), indicating the suppressive function of *Am*TARS on pro-inflammatory responses *in vivo*.

Engineered *Ec*N-secreting *Am*TARS significantly ameliorates inflammation in mice with colitis

The bacterium *E. coli* Nissle 1917 (*Ec*N) is a well-known probiotic that has intrinsic antibacterial and anti-inflammatory properties.[58] *Ec*N is fast emerging as a candidate for development as a therapeutically engineered bacterium.[59] Therefore, we engineered this bacterium to further validate the physiological function of *Am*TARS *in vivo*. First, we tried to engineer *Ec*N to create an *Am*TARS-secreting bacterium by chromosomally replacing *Ec*N TARS with *Am*TARS. However, this replacement was lethal to *Ec*N because the cognate tRNAs of *Ec*N TARS required for amino-acylation may be not compatible with *Am*TARS. Note that ARSs are highly specific with respect to selecting their cognate amino acids and tRNA substrates and have distinct modes of recognition in different organisms. Therefore, we next developed a chromosomally engineered *Ec*N that contains additional TARS (i.e., *Am*TARS) expressed ectopically at different locations of the chromosome. The *Am*TARS gene and the *lac* promoter were inserted into the *exo*/*cea* convergent intergenic region, which has been exploited previously in other studies[60,61]; therefore, it does not interfere with the expression of neighboring genes (Figure S6C). A 6X His tag was added to the C terminus of *Am*TARS for use in further analyses. It should be noted that no signal peptide sequence was added to *Am*TARS in the engineered *Ec*N; this is because the original *Am*TARS also does not have one. Indeed, secretion of ARSs for non-translational functions has been observed in humans, although the mechanism is unknown.[18,19,21,62]

The engineered *Ec*N (*Ec*N(AmTARS)) was secreted *Am*TARS extracellularly at significantly lower levels than *A. muciniphila*; indeed, the amount of *Am*TARS in a 40-fold-concentrated culture supernatant from *Ec*N(AmTARS) was the same as that secreted by *A. muciniphila* (Figure 7A). Subsequently, we used the His tag to evaluate *Am*TARS secreted by the engineered bacterium in the colon of mice with DSS-induced colitis orally administered with *Ec*N(AmTARS). Immunofluorescence staining clearly showed that most of the engineered *Ec*N-secreting *Am*TARSs (His) co-localized with macrophages (F4/80-positive) located in the lamina propria of the colon (Figures 7B and 7C), confirming that *Am*TARS targets macrophages in the gut.

Oral administration of *Ec*N(AmTARS) significantly improved colitis-induced body weight loss, shortening of colon length, disease activity scores, disruption of the epithelial lining, and damage score (Figures 7D–7F, S6D, and S6E). In addition, it significantly reduced colitis-induced infiltration by inflammatory monocytes, restored IL-10-secreting macrophages, and markedly increased IL-10 levels in the serum of colitis mice (Figures 7G–7I).

Taken together, these data provide further evidence that *Am*TARS secreted by the commensal bacterium *A. muciniphila* is a steady-state immune homeostatic mediator that is distinct from typical TLR2 ligands and which maintains and induces immune homeostasis via the modulation of residential macrophages in the gut in response to inflammatory challenges (Figure 7J).

DISCUSSION

Over 10^{13} bacteria reside in the human gut, forming a mutual relationship with the host that confers many benefits,

(H and I) *Am*TARS activates both TLR2/1- and TLR2/6-mediated signaling. Activation of AKT, ERK, and CREB was measured by western blot analysis of lysates of THP1 cells (H), and IL-10 in BMDM culture supernatant was detected by ELISA (n = 6 per group) (I). The cells were pre-treated with α-IgG, α-TLR1, α-TLR2, or α-TLR6 (1 μg mL^{-1}) for 1 h before treatment for 30 min (H) or 24 h (I) with PBS or *Am*TARS (0.5 μM).

Data shown in (A), (B), and (I) are representative of three independent experiments, each with similar results (mean ± SEM). p values were calculated using an unpaired two-tailed Student's t test. Data shown in (C)–(H) are representative of three independent experiments.

CellPress
OPEN ACCESS

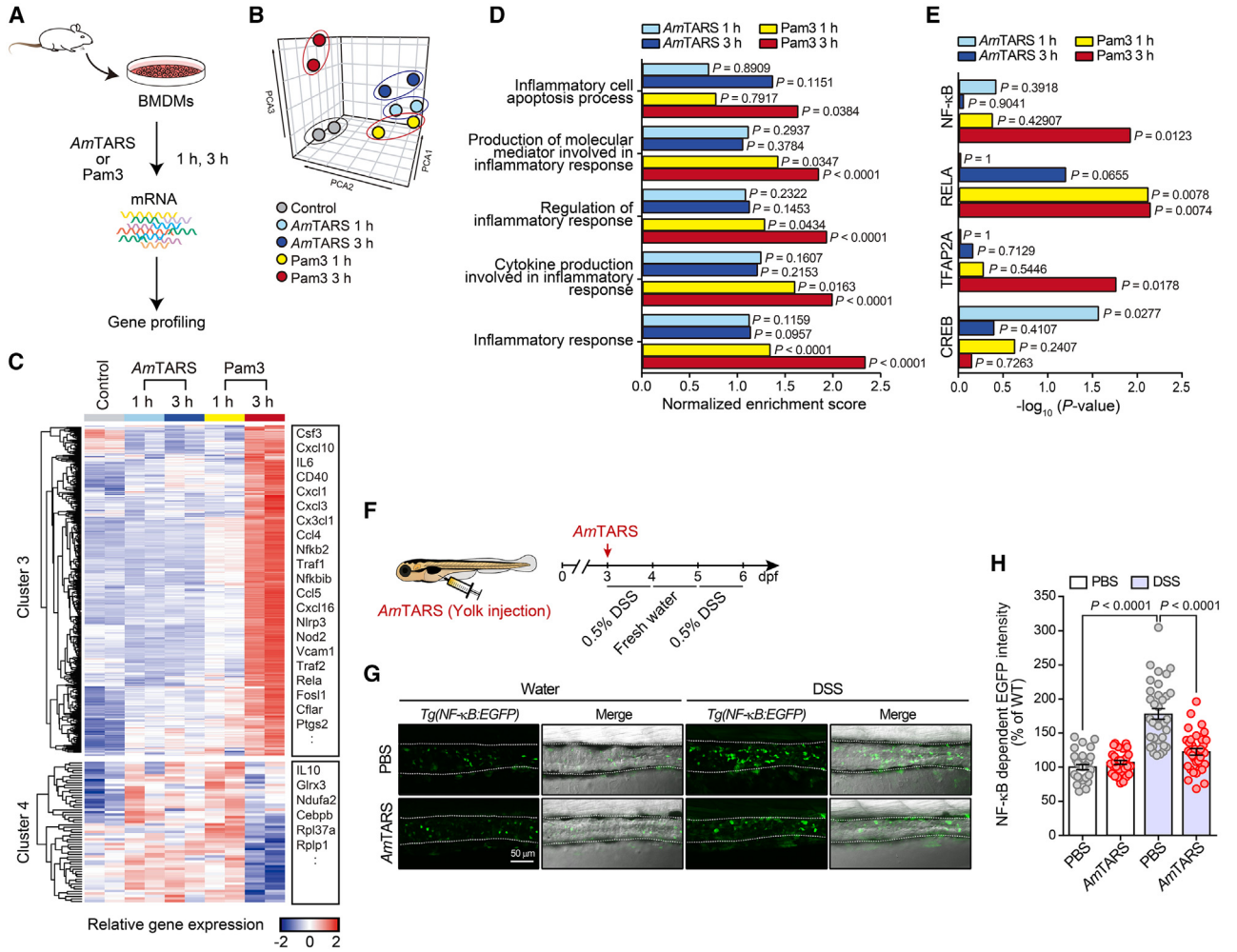

Figure 6. *Am*TARS is a steady-state, immune homeostatic mediator

(A–E) Global gene expression analysis. Total mRNA from BMDMs treated with either *Am*TARS (0.5 μM) or Pam3 (10 ng mL^{-1}) for 1 or 3 h was isolated and analyzed by RNA sequencing (A). Principal-component analysis (PCA) of the gene expression profiles for each sample (B). Hierarchical clustering of gene expression profiles from each sample identified cluster 3 and 4 (C). The complete gene sets are shown in Figure S6A. Gene set enrichment analysis (GSEA) of clusters 3 and 4 with respect to terms related to inflammation (D). GSEA was performed for upregulated genes using Enrichr to identify terms associated with transcription factors (E).

(F) Overview of the experimental procedures for zebrafish. The yolk of *Tg(NFκB:EGFP)* transgenic zebrafish larvae (3 dpf) was injected with PBS or *Am*TARS. Injected larvae were treated at 3 and 5 dpf with 0.5% DSS for 24 h, with a washing period with fresh water for 24 h in between. Sample collection and analysis of *Tg(NFκB:EGFP)*-based EGFP intensity were conducted at 6 dpf.

(G) Representative confocal images showing NF-κB signaling in the mid-distal intestines of PBS- or *Am*TARS-injected larvae with or without DSS treatment. White-dashed lines denote the boundaries of the intestines (based on merged DIC bright-field images).

(H) Bar graph comparing the fluorescence intensity of the mid-distal intestines of PBS- or *Am*TARS-injected larvae treated (or not) with DSS (n = 32 per PBS group and n = 35 per DSS group).

Data shown in (A)–(C) are representative of two independent experiments. Data shown in (H) are representative of three independent experiments, each similar results (mean ± SEM). p values were calculated by unpaired and two-tailed Student's t test.

particularly in relation to intestinal physiology.[63,64] Failure to shape gut immune activity results in deregulated and excessive inflammatory responses that are linked to chronic inflammatory disorders such as IBDs.[5–7] Although it is well appreciated that diet-dependent nutrients and metabolites such as short-chain fatty acids derived from commensals are important regulators of host immunity,[8,9] the involvement of the biological systems of commensals themselves remains unexplored.

The immune system, which can discriminate between beneficial commensals and pathogens, as well as recognize dietary antigens, balances immune responses and tolerance to maintain intestinal homeostasis.[65,66] Under normal steady-state conditions, TLRs play an important role in these events by sensing commensal bacteria.[45] The anti-inflammatory cytokine IL-10 and its major producer macrophages are crucial players in maintaining intestinal homeostasis.[67–71] Thus, the interplay between commensals, TLRs, and IL-10 may be a critical axis that

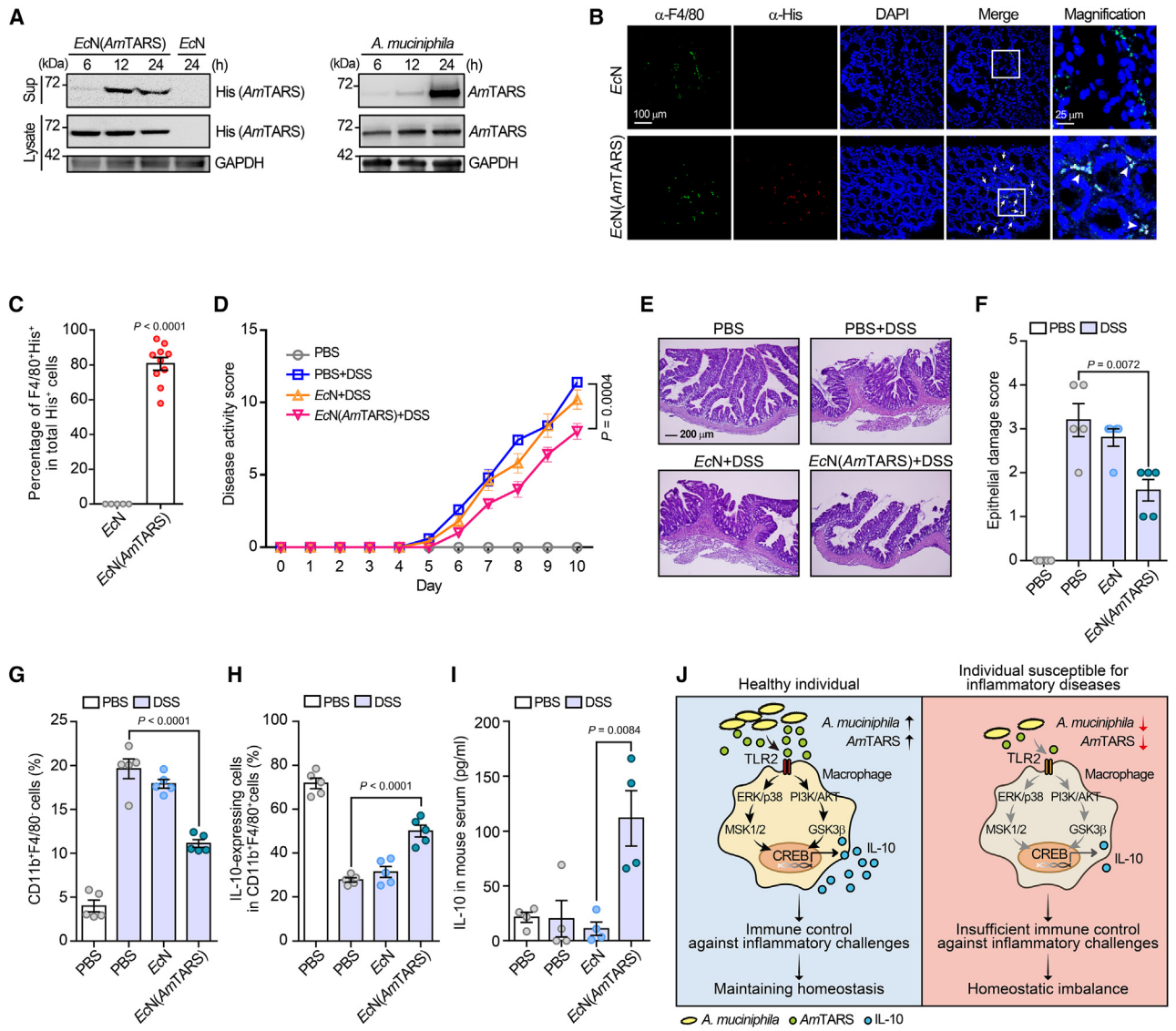

Figure 7. Oral administration of *Ec*N(AmTARS) alleviates DSS-induced colitis

(A) Western blot analysis of engineered *Ec*N- or *A. muciniphila*-secreted *Am*TARS. GAPDH was used as a control.

(B and C) Immunofluorescence staining (using *Am*TARS (His)) of macrophages (F4/80-positive) from the colon obtained from DSS-induced colitis mice orally administered (10^7 per mouse) daily with *Ec*N or *Ec*N(AmTARS) for 5 days (B), and the percentage of $F4/80^+His^+$ cells among the total His^+ cells in (B) (n = 5 per *Ec*N group and n = 10 per *Ec*N(AmTARS) group) (C).

(D–I) DSS-induced colitis mice orally administered (10^7 per mouse) daily with *Ec*N or *Ec*N(AmTARS) (n = 5 per group). Measurement of the disease activity score (D) and intestinal epithelial damage, as analyzed by H&E staining of the proximal colon (E), and damage scores (F). Percentage of infiltrated immune cells, gated on $CD11b^+F4/80^-$ (monocytes) (G) and $CD11b^+F4/80^+IL\text{-}10^+$ (IL-10-secreting macrophages) (H). IL-10 levels in mouse serum (n = 4 per group) (I).

(J) Schematic model of the role of *Am*TARS in maintaining immune homeostasis via TLR2-mediated anti-inflammatory signaling pathways.

Data shown in (A), (B), and (E) are representative of three independent experiments. Data shown in (C), (D), and (F)–(I) are representative of three independent experiments, each with similar results (mean ± SEM). p values were calculated by an unpaired two-tailed Student's t test.

instigates and shapes the immune responses required for homeostatic balance in an environment that is exposed constantly to inflammatory challenges. Moreover, the key modulator in this intricate interplay has yet to be identified.

Generally speaking, TLR2 recognizes classical bacterial constituents such as lipopeptides and lipoteichoic acid and initiates innate immune responses, including NF-κB-mediated inflammation, that are necessary for host protection.[72] A recent study shows that TLR2 also recognizes a large soluble polysaccharide produced by *Helicobacter hepaticus*, a member of the mouse intestinal microbiota.[51] Polysaccharide-sensing TLR2 triggers MSK/CREB signaling in intestinal macrophages, thereby inducing an early production of IL-10 and promoting tolerance to inflammatory challenges. The TLR2 ligand polysaccharide functions differently from the typical ligand Pam3; indeed, it failed to induce the production of IL-10 by *Tlr2*$^{-/-}$ BMDMs but

not by WT, Tlr1$^{-/-}$, and Tlr6$^{-/-}$ cells. Another representative example of a gut commensal-associated immune tolerance event triggered via TLR2 is mediated by *Bacteroides fragilis*-secreted polysaccharide A (PSA). Unlike typical TLR2 ligands such as Pam3, secreted PSA promotes IL-10 production by activating CD4$^+$ T cells through TLR2.[65] *B. fragilis*-secreted PSA induces high amounts of IL-10 production by WT, Tlr1$^{-/-}$, and Tlr6$^{-/-}$ CD4$^+$ T cells but not by *Tlr2*$^{-/-}$ cells.[65]

Here, we report that *A. muciniphila* exhibits steady-state secretion of an immune mediator, *Am*TARS, which acts as a TLR2-specific ligand to monitor and induce immune homeostasis to protect against inflammatory challenges. Like PSA and soluble polysaccharides, *Am*TARS triggers anti-inflammatory immune signaling, although it seems to function differently from those ligands. Although the TLR-deficient cell experiments suggest that both *B. fragilis*-secreted PSA and *H. hepaticus*-produced soluble polysaccharide target only the homodimeric TLR2 form, *Am*TARS targets the TLR2/2, TLR2/1, and TLR2/6 forms to trigger anti-inflammatory signaling (Figures 5H and 5I). The distinctiveness of *Am*TARS with respect to specificity for TLR2 may allow efficient induction of immune homeostasis via activation of CREB through both the MAPK and PI3K/AKT signaling pathways. Thus, these experiments reveal a gut inhabitant that actively stimulates mutualistic interactions with its host to maintain intestinal homeostasis via anti-inflammatory TLR signaling. In addition, these studies suggest that TLR2 may act as the main receptor that maintains intestinal homeostasis by communicating with resident commensals.

The anaerobic bacterium *A. muciniphila* is the only known species of the *Verrucomicrobia* phylum that resides in the gastrointestinal tract of humans and animals,[73] and the abundance of this organism correlates inversely with metabolic and inflammatory disorders.[37–40] In general, members of the *Verrucomicrobia* phylum encode enzymes required for synthesis of threonine from homoserine; however, genes encoding these enzymes are absent from the *A. muciniphila* genome, despite L-threonine being essential for its growth.[74,75] Adaptation of this bacterium to the mucosal environment may be a consequence of its threonine auxotrophy since this amino acid is abundant in mucin.[76] It is noteworthy that *A. muciniphila* is capable of producing an extensive repertoire of mucin-degrading enzymes.[74] The canonical function of *Am*TARS is to catalyze intracellular covalent ligation of threonine to a corresponding tRNA for protein synthesis. We speculate that steady-state secretion of *Am*TARS may be related to the organism's threonine auxotrophy but that it may concomitantly allow surveillance of gut immune status. This hypothesis remains to be proven conclusively. Nevertheless, our findings highlight an exquisite, interdependent relationship between *A. muciniphila* and the gut environment, which contributes to host immune homeostasis.

The incidence of IBD is increasing rapidly worldwide; indeed, IBD has become a globally emerging disease.[77,78] It is now clear that altered gut microbiota, or aberrant immune responses to the microbiota, play crucial roles in the pathogenesis of IBD.[36,79] IL-10 acts is a key player in the maintenance of gut homeostasis[69,80,81]; as such, it is considered to be a potential therapeutic treatment for IBD.[82] Since *Am*TARS functions as an anti-inflammatory immune mediator, leading to the production of IL-10, we propose that it may serve as a biomarker and potential therapeutic agent for IBD. Indeed, the therapeutic effects of *Am*TARS on colitis pathology including body weight loss, disease activity score, shortening of the colon length, disruption of the epithelial lining, and the damage score were comparable with those of IL-10 in mice with colitis (Figures S7A–S7E). *Am*TARS reduced colitis-induced infiltration by inflammatory monocytes similar to IL-10 (Figures S7F and S7G). In addition, because systemically administered *Am*TARS modulates intestinal inflammation, it might also be able to control systemic inflammation in diseases such as rheumatoid arthritis and systemic lupus erythematosus.

In summary, this study demonstrates that commensal ARS plays a critical role in the maintenance of immune homeostasis by triggering steady-state IL-10-mediated anti-inflammatory immune regulation. Simultaneously, our study provides a unique perspective of gut microbiota–host mutualism, in which commensal ARSs may act as intrinsic mediators that shape holobiont homeostasis. Thus, our findings may lead to strategies for the prevention and therapeutic treatment of various inflammatory diseases, including IBD.

STAR★METHODS

Detailed methods are provided in the online version of this paper and include the following:

- KEY RESOURCES TABLE
- RESOURCE AVAILABILITY
  - Lead contact
  - Materials availability
  - Data and code availability
- EXPERIMENTAL MODEL AND SUBJECT DETAILS
  - Mice
  - Isolation of primary cells
  - HEK293T cell lines
  - THP-1 cell line
  - *A. muciniphila* culture
  - Zebrafish husbandry
- METHOD DETAILS
  - Induction of DSS-induced colitis and measurement of disease activity
  - H&E and immunofluorescence staining
  - Flow cytometry
  - Gene cloning
  - Immunoblotting
  - Protein expression and purification
  - Interactome analysis
  - Pull-down assay
  - *In vitro* binding assay
  - Enzyme-linked immunosorbent assay (ELISA)
  - Isolation of *A. muciniphila* EV
  - LC-MS/MS analysis of soluble fractions and EVs from *A. muciniphila*
  - DSS-induced zebrafish colitis model
  - Confocal microscopy analysis of intestinal NF-κB activity
  - Antibody production
  - Amino-acylation assay
  - Construction of the engineered *Ec*N strain
  - Adoptive cell transfer

SUPPLEMENTAL INFORMATION

Supplemental information can be found online at https://doi.org/10.1016/j.chom.2023.05.007.

ACKNOWLEDGMENTS

This work is supported by grants from National Research Foundation of Korea (2015M3C9A4053394 to M.H.K.; 2015R1A3A2033475 and 2022M3A9F3082326 to W.-J.L.) funded by the Ministry of Science and ICT, and by the KRIBB Research Initiative Program (KGM1382312 to M.H.K.).

AUTHOR CONTRIBUTIONS

M.H.K. conceived and supervised the project. S.-M.K. designed and carried out all animal experiments with the help of S.P., J.-H.K., T.-H.K., and C.-H.L. S.P. designed and carried out biochemical, cell biological, and immunological analysis with the help of S.-M.K. and E.-Y.L. S.-H.H. engineered *E. coli* Nissle secreting *Am*TARS with the help of M.K. and E.-K.K. S.-M.K., J.-H.K., and S.-Y.K. carried out transcriptomic analysis. G.S.L. and J.H.M. performed the LC/MS experiments for interactome analysis. G.L. and G.K. performed metagenomic and metatranscriptomic analysis of bacterial aminoacyl-tRNA synthetases using iHMP datasets. D.-H.C. and B.-C.K. performed anaerobic culture experiments using *A. muciniphila*. J.H. and Y.L. performed structure modeling of *Am*TARS. J.-G.L. and J.-S.L. conducted experiments on zebrafish. S.-M.K., S.P., J.-H.R., J.-Y.K., S.K., W.-J.L., and M.H.K. analyzed and interpreted the data. S.-M.K. and S.P. drafted the manuscript, and M.H.K. edited the manuscript, with input from all authors.

DECLARATION OF INTERESTS

The authors declare no competing interests.

Received: July 23, 2022
Revised: March 23, 2023
Accepted: May 9, 2023
Published: June 2, 2023

REFERENCES

1. O'Hara, A.M., and Shanahan, F. (2006). The gut flora as a forgotten organ. EMBO Rep. *7*, 688–693. https://doi.org/10.1038/sj.embor.7400731.
2. Sommer, F., and Bäckhed, F. (2013). The gut microbiota–masters of host development and physiology. Nat. Rev. Microbiol. *11*, 227–238. https://doi.org/10.1038/nrmicro2974.
3. Turnbaugh, P.J., Hamady, M., Yatsunenko, T., Cantarel, B.L., Duncan, A., Ley, R.E., Sogin, M.L., Jones, W.J., Roe, B.A., Affourtit, J.P., et al. (2009). A core gut microbiome in obese and lean twins. Nature *457*, 480–484. https://doi.org/10.1038/nature07540.
4. Zheng, D., Liwinski, T., and Elinav, E. (2020). Interaction between microbiota and immunity in health and disease. Cell Res. *30*, 492–506. https://doi.org/10.1038/s41422-020-0332-7.
5. Fan, Y., and Pedersen, O. (2021). Gut microbiota in human metabolic health and disease. Nat. Rev. Microbiol. *19*, 55–71. https://doi.org/10.1038/s41579-020-0433-9.
6. Levy, M., Kolodziejczyk, A.A., Thaiss, C.A., and Elinav, E. (2017). Dysbiosis and the immune system. Nat. Rev. Immunol. *17*, 219–232. https://doi.org/10.1038/nri.2017.7.
7. Human Microbiome Project Consortium (2012). Structure, function and diversity of the healthy human microbiome. Nature *486*, 207–214. https://doi.org/10.1038/nature11234.
8. Brestoff, J.R., and Artis, D. (2013). Commensal bacteria at the interface of host metabolism and the immune system. Nat. Immunol. *14*, 676–684. https://doi.org/10.1038/ni.2640.
9. Postler, T.S., and Ghosh, S. (2017). Understanding the holobiont: how microbial metabolites affect human health and shape the immune system. Cell Metab. *26*, 110–130. https://doi.org/10.1016/j.cmet.2017.05.008.
10. Rooks, M.G., and Garrett, W.S. (2016). Gut microbiota, metabolites and host immunity. Nat. Rev. Immunol. *16*, 341–352. https://doi.org/10.1038/nri.2016.42.
11. Belkaid, Y., and Hand, T.W. (2014). Role of the microbiota in immunity and inflammation. Cell *157*, 121–141. https://doi.org/10.1016/j.cell.2014.03.011.
12. Ibba, M., and Söll, D. (2001). The renaissance of aminoacyl-tRNA synthesis. EMBO Rep. *2*, 382–387. https://doi.org/10.1093/embo-reports/kve095.
13. Kwon, N.H., Fox, P.L., and Kim, S. (2019). Aminoacyl-tRNA synthetases as therapeutic targets. Nat. Rev. Drug Discov. *18*, 629–650. https://doi.org/10.1038/s41573-019-0026-3.
14. Yao, P., and Fox, P.L. (2013). Aminoacyl-tRNA synthetases in medicine and disease. EMBO Mol. Med. *5*, 332–343. https://doi.org/10.1002/emmm.201100626.
15. Guo, M., and Schimmel, P. (2013). Essential nontranslational functions of tRNA synthetases. Nat. Chem. Biol. *9*, 145–153. https://doi.org/10.1038/nchembio.1158.
16. Guo, M., Yang, X.L., and Schimmel, P. (2010). New functions of aminoacyl-tRNA synthetases beyond translation. Nat. Rev. Mol. Cell Biol. *11*, 668–674. https://doi.org/10.1038/nrm2956.
17. Kim, M.H., and Kim, S. (2020). Structures and functions of multi-tRNA synthetase complexes. Enzymes *48*, 149–173. https://doi.org/10.1016/bs.enz.2020.06.008.
18. Cho, S., Kim, S.B., Lee, Y., Song, E.C., Kim, U., Kim, H.Y., Suh, J.H., Goughnour, P.C., Kim, Y., Yoon, I., et al. (2020). Endogenous TLR2 ligand embedded in the catalytic region of human cysteinyl-tRNA synthetase 1. J. Immunother. Cancer *8*. https://doi.org/10.1136/jitc-2019-000277.
19. Ahn, Y.H., Park, S., Choi, J.J., Park, B.K., Rhee, K.H., Kang, E., Ahn, S., Lee, C.H., Lee, J.S., Inn, K.S., et al. (2016). Secreted tryptophanyl-tRNA synthetase as a primary defence system against infection. Nat. Microbiol. *2*, 16191. https://doi.org/10.1038/nmicrobiol.2016.191.
20. Kim, S.B., Kim, H.R., Park, M.C., Cho, S., Goughnour, P.C., Han, D., Yoon, I., Kim, Y., Kang, T., Song, E., et al. (2017). Caspase-8 controls the secretion of inflammatory lysyl-tRNA synthetase in exosomes from cancer cells. J. Cell Biol. *216*, 2201–2216. https://doi.org/10.1083/jcb.201605118.
21. Williams, T.F., Mirando, A.C., Wilkinson, B., Francklyn, C.S., and Lounsbury, K.M. (2013). Secreted threonyl-tRNA synthetase stimulates endothelial cell migration and angiogenesis. Sci. Rep. *3*, 1317. https://doi.org/10.1038/srep01317.
22. Collado, M.C., Derrien, M., Isolauri, E., de Vos, W.M., and Salminen, S. (2007). Intestinal integrity and Akkermansia muciniphila, a mucin-degrading member of the intestinal microbiota present in infants, adults, and the elderly. Appl. Environ. Microbiol. *73*, 7767–7770. https://doi.org/10.1128/AEM.01477-07.
23. Cani, P.D., Depommier, C., Derrien, M., Everard, A., and de Vos, W.M. (2022). Akkermansia muciniphila: paradigm for next-generation beneficial microorganisms. Nat. Rev. Gastroenterol. Hepatol. *19*, 625–637. https://doi.org/10.1038/s41575-022-00631-9.
24. Shin, J., Noh, J.R., Choe, D., Lee, N., Song, Y., Cho, S., Kang, E.J., Go, M.J., Ha, S.K., Chang, D.H., et al. (2021). Ageing and rejuvenation models reveal changes in key microbial communities associated with healthy

ageing. Microbiome *9*, 240. https://doi.org/10.1186/s40168-021-01189-5.

25. Greer, R.L., Dong, X., Moraes, A.C., Zielke, R.A., Fernandes, G.R., Peremyslova, E., Vasquez-Perez, S., Schoenborn, A.A., Gomes, E.P., Pereira, A.C., et al. (2016). Akkermansia muciniphila mediates negative effects of IFNgamma on glucose metabolism. Nat. Commun. *7*, 13329. https://doi.org/10.1038/ncomms13329.
26. Yoon, H.S., Cho, C.H., Yun, M.S., Jang, S.J., You, H.J., Kim, J.H., Han, D., Cha, K.H., Moon, S.H., Lee, K., et al. (2021). Akkermansia muciniphila secretes a glucagon-like peptide-1-inducing protein that improves glucose homeostasis and ameliorates metabolic disease in mice. Nat. Microbiol. *6*, 563–573. https://doi.org/10.1038/s41564-021-00880-5.
27. Basolo, A., Hohenadel, M., Ang, Q.Y., Piaggi, P., Heinitz, S., Walter, M., Walter, P., Parrington, S., Trinidad, D.D., von Schwartzenberg, R.J., et al. (2020). Effects of underfeeding and oral vancomycin on gut microbiome and nutrient absorption in humans. Nat. Med. *26*, 589–598. https://doi.org/10.1038/s41591-020-0801-z.
28. Bárcena, C., Valdés-Mas, R., Mayoral, P., Garabaya, C., Durand, S., Rodríguez, F., Fernández-García, M.T., Salazar, N., Nogacka, A.M., Garatachea, N., et al. (2019). Healthspan and lifespan extension by fecal microbiota transplantation into progeroid mice. Nat. Med. *25*, 1234–1242. https://doi.org/10.1038/s41591-019-0504-5.
29. Plovier, H., Everard, A., Druart, C., Depommier, C., Van Hul, M., Geurts, L., Chilloux, J., Ottman, N., Duparc, T., Lichtenstein, L., et al. (2017). A purified membrane protein from Akkermansia muciniphila or the pasteurized bacterium improves metabolism in obese and diabetic mice. Nat. Med. *23*, 107–113. https://doi.org/10.1038/nm.4236.
30. Ansaldo, E., Slayden, L.C., Ching, K.L., Koch, M.A., Wolf, N.K., Plichta, D.R., Brown, E.M., Graham, D.B., Xavier, R.J., Moon, J.J., et al. (2019). Akkermansia muciniphila induces intestinal adaptive immune responses during homeostasis. Science *364*, 1179–1184. https://doi.org/10.1126/science.aaw7479.
31. Kuehn, M.J., and Kesty, N.C. (2005). Bacterial outer membrane vesicles and the host-pathogen interaction. Genes Dev. *19*, 2645–2655. https://doi.org/10.1101/gad.1299905.
32. Kang, C.S., Ban, M., Choi, E.J., Moon, H.G., Jeon, J.S., Kim, D.K., Park, S.K., Jeon, S.G., Roh, T.Y., Myung, S.J., et al. (2013). Extracellular vesicles derived from gut microbiota, especially Akkermansia muciniphila, protect the progression of dextran sulfate sodium-induced colitis. PLoS One *8*, e76520. https://doi.org/10.1371/journal.pone.0076520.
33. McGovern, D.P., Kugathasan, S., and Cho, J.H. (2015). Genetics of inflammatory bowel diseases. Gastroenterology *149,* 1163–1176.e2. https://doi.org/10.1053/j.gastro.2015.08.001.
34. Piovani, D., Danese, S., Peyrin-Biroulet, L., Nikolopoulos, G.K., Lytras, T., and Bonovas, S. (2019). Environmental risk factors for inflammatory bowel diseases: an umbrella review of meta-analyses. Gastroenterology *157,* 647–659.e4. https://doi.org/10.1053/j.gastro.2019.04.016.
35. Parada Venegas, D., De la Fuente, M.K., Landskron, G., González, M.J., Quera, R., Dijkstra, G., Harmsen, H.J.M., Faber, K.N., and Hermoso, M.A. (2019). Short chain fatty acids (SCFAs)-mediated gut epithelial and immune regulation and its relevance for inflammatory bowel diseases. Front. Immunol. *10*, 277. https://doi.org/10.3389/fimmu.2019.00277.
36. Lloyd-Price, J., Arze, C., Ananthakrishnan, A.N., Schirmer, M., Avila-Pacheco, J., Poon, T.W., Andrews, E., Ajami, N.J., Bonham, K.S., Brislawn, C.J., et al. (2019). Multi-omics of the gut microbial ecosystem in inflammatory bowel diseases. Nature *569*, 655–662. https://doi.org/10.1038/s41586-019-1237-9.
37. Depommier, C., Everard, A., Druart, C., Plovier, H., Van Hul, M., Vieira-Silva, S., Falony, G., Raes, J., Maiter, D., Delzenne, N.M., et al. (2019). Supplementation with Akkermansia muciniphila in overweight and obese human volunteers: a proof-of-concept exploratory study. Nat. Med. *25*, 1096–1103. https://doi.org/10.1038/s41591-019-0495-2.
38. Yassour, M., Lim, M.Y., Yun, H.S., Tickle, T.L., Sung, J., Song, Y.M., Lee, K., Franzosa, E.A., Morgan, X.C., Gevers, D., et al. (2016). Sub-clinical detection of gut microbial biomarkers of obesity and type 2 diabetes. Genome Med. *8*, 17. https://doi.org/10.1186/s13073-016-0271-6.
39. Dao, M.C., Everard, A., Aron-Wisnewsky, J., Sokolovska, N., Prifti, E., Verger, E.O., Kayser, B.D., Levenez, F., Chilloux, J., Hoyles, L., et al. (2016). Akkermansia muciniphila and improved metabolic health during a dietary intervention in obesity: relationship with gut microbiome richness and ecology. Gut *65*, 426–436. https://doi.org/10.1136/gutjnl-2014-308778.
40. Wang, L., Tang, L., Feng, Y., Zhao, S., Han, M., Zhang, C., Yuan, G., Zhu, J., Cao, S., Wu, Q., et al. (2020). A purified membrane protein from Akkermansia muciniphila or the pasteurised bacterium blunts colitis associated tumourigenesis by modulation of CD8(+) T cells in mice. Gut *69*, 1988–1997. https://doi.org/10.1136/gutjnl-2019-320105.
41. Mantovani, A., Sica, A., Sozzani, S., Allavena, P., Vecchi, A., and Locati, M. (2004). The chemokine system in diverse forms of macrophage activation and polarization. Trends Immunol. *25*, 677–686. https://doi.org/10.1016/j.it.2004.09.015.
42. Martinez, F.O., Helming, L., and Gordon, S. (2009). Alternative activation of macrophages: an immunologic functional perspective. Annu. Rev. Immunol. *27*, 451–483. https://doi.org/10.1146/annurev.immunol.021908.132532.
43. Jumper, J., Evans, R., Pritzel, A., Green, T., Figurnov, M., Ronneberger, O., Tunyasuvunakool, K., Bates, R., Žídek, A., Potapenko, A., et al. (2021). Highly accurate protein structure prediction with AlphaFold. Nature *596*, 583–589. https://doi.org/10.1038/s41586-021-03819-2.
44. Janeway, C.A., Jr., and Medzhitov, R. (2002). Innate immune recognition. Annu. Rev. Immunol. *20*, 197–216. https://doi.org/10.1146/annurev.immunol.20.083001.084359.
45. Rakoff-Nahoum, S., Paglino, J., Eslami-Varzaneh, F., Edberg, S., and Medzhitov, R. (2004). Recognition of commensal microflora by toll-like receptors is required for intestinal homeostasis. Cell *118*, 229–241. https://doi.org/10.1016/j.cell.2004.07.002.
46. Lang, T., and Mansell, A. (2007). The negative regulation of toll-like receptor and associated pathways. Immunol. Cell Biol. *85*, 425–434. https://doi.org/10.1038/sj.icb.7100094.
47. Liew, F.Y., Xu, D., Brint, E.K., and O'Neill, L.A. (2005). Negative regulation of toll-like receptor-mediated immune responses. Nat. Rev. Immunol. *5*, 446–458. https://doi.org/10.1038/nri1630.
48. Saraiva, M., and O'Garra, A. (2010). The regulation of IL-10 production by immune cells. Nat. Rev. Immunol. *10*, 170–181. https://doi.org/10.1038/nri2711.
49. Wen, A.Y., Sakamoto, K.M., and Miller, L.S. (2010). The role of the transcription factor CREB in immune function. J. Immunol. *185*, 6413–6419. https://doi.org/10.4049/jimmunol.1001829.
50. Sanin, D.E., Prendergast, C.T., and Mountford, A.P. (2015). IL-10 production in macrophages is regulated by a TLR-driven CREB-mediated mechanism that is linked to genes involved in cell metabolism. J. Immunol. *195*, 1218–1232. https://doi.org/10.4049/jimmunol.1500146.
51. Danne, C., Ryzhakov, G., Martínez-López, M., Ilott, N.E., Franchini, F., Cuskin, F., Lowe, E.C., Bullers, S.J., Arthur, J.S.C., and Powrie, F. (2017). A large polysaccharide Produced by Helicobacter hepaticus Induces an Anti-inflammatory Gene Signature in Macrophages. Cell Host Microbe *22,* 733–745.e5. https://doi.org/10.1016/j.chom.2017.11.002.
52. Ananieva, O., Darragh, J., Johansen, C., Carr, J.M., McIlrath, J., Park, J.M., Wingate, A., Monk, C.E., Toth, R., Santos, S.G., et al. (2008). The kinases MSK1 and MSK2 act as negative regulators of toll-like receptor signaling. Nat. Immunol. *9*, 1028–1036. https://doi.org/10.1038/ni.1644.
53. Ollivier, V., Parry, G.C., Cobb, R.R., de Prost, D., and Mackman, N. (1996). Elevated cyclic AMP inhibits NF-kappaB-mediated transcription in human monocytic cells and endothelial cells. J. Biol. Chem. *271*, 20828–20835. https://doi.org/10.1074/jbc.271.34.20828.

54. Parry, G.C., and Mackman, N. (1997). Role of cyclic AMP response element-binding protein in cyclic AMP inhibition of NF-kappaB-mediated transcription. J. Immunol. *159*, 5450–5456.

55. Martin, M., Rehani, K., Jope, R.S., and Michalek, S.M. (2005). Toll-like receptor-mediated cytokine production is differentially regulated by glycogen synthase kinase 3. Nat. Immunol. *6*, 777–784. https://doi.org/10.1038/ni1221.

56. Lee, W.B., Kang, J.S., Choi, W.Y., Zhang, Q., Kim, C.H., Choi, U.Y., Kim-Ha, J., and Kim, Y.J. (2016). Mincle-mediated translational regulation is required for strong nitric oxide production and inflammation resolution. Nat. Commun. *7*, 11322. https://doi.org/10.1038/ncomms11322.

57. Lee, J.G., Lee, S., Jeon, J., Kong, H.G., Cho, H.J., Kim, J.H., Kim, S.Y., Oh, M.J., Lee, D., Seo, N., et al. (2022). Host tp53 mutation induces gut dysbiosis eliciting inflammation through disturbed sialic acid metabolism. Microbiome *10*, 3. https://doi.org/10.1186/s40168-021-01191-x.

58. Lynch, J.P., Goers, L., and Lesser, C.F. (2022). Emerging strategies for engineering Escherichia coli Nissle 1917-based therapeutics. Trends Pharmacol. Sci. *43*, 772–786. https://doi.org/10.1016/j.tips.2022.02.002.

59. Sonnenborn, U. (2016). Escherichia coli strain Nissle 1917-from bench to bedside and back: history of a special Escherichia coli strain with probiotic properties. FEMS Microbiol. Lett. *363*. https://doi.org/10.1093/femsle/fnw212.

60. Isabella, V.M., Ha, B.N., Castillo, M.J., Lubkowicz, D.J., Rowe, S.E., Millet, Y.A., Anderson, C.L., Li, N., Fisher, A.B., West, K.A., et al. (2018). Development of a synthetic live bacterial therapeutic for the human metabolic disease phenylketonuria. Nat. Biotechnol. *36*, 857–864. https://doi.org/10.1038/nbt.4222.

61. Leventhal, D.S., Sokolovska, A., Li, N., Plescia, C., Kolodziej, S.A., Gallant, C.W., Christmas, R., Gao, J.R., James, M.J., Abin-Fuentes, A., et al. (2020). Immunotherapy with engineered bacteria by targeting the STING pathway for anti-tumor immunity. Nat. Commun. *11*, 2739. https://doi.org/10.1038/s41467-020-16602-0.

62. Zhou, J.J., Wang, F., Xu, Z., Lo, W.S., Lau, C.F., Chiang, K.P., Nangle, L.A., Ashlock, M.A., Mendlein, J.D., Yang, X.L., et al. (2014). Secreted histidyl-tRNA synthetase splice variants elaborate major epitopes for autoantibodies in inflammatory myositis. J. Biol. Chem. *289*, 19269–19275. https://doi.org/10.1074/jbc.C114.571026.

63. Sender, R., Fuchs, S., and Milo, R. (2016). Are we really vastly outnumbered? Revisiting the ratio of bacterial to host cells in humans. Cell *164*, 337–340. https://doi.org/10.1016/j.cell.2016.01.013.

64. Hooper, L.V., and Gordon, J.I. (2001). Commensal host-bacterial relationships in the gut. Science *292*, 1115–1118. https://doi.org/10.1126/science.1058709.

65. Round, J.L., Lee, S.M., Li, J., Tran, G., Jabri, B., Chatila, T.A., and Mazmanian, S.K. (2011). The toll-like receptor 2 pathway establishes colonization by a commensal of the human microbiota. Science *332*, 974–977. https://doi.org/10.1126/science.1206095.

66. Rodriguez-Sillke, Y., Visekruna, A., Glauben, R., Siegmund, B., and Steinhoff, U. (2021). Recognition of food antigens by the mucosal and systemic immune system: consequences for intestinal development and homeostasis. Int. J. Med. Microbiol. *311*, 151493. https://doi.org/10.1016/j.ijmm.2021.151493.

67. Mantovani, A., and Marchesi, F. (2014). IL-10 and macrophages orchestrate gut homeostasis. Immunity *40*, 637–639. https://doi.org/10.1016/j.immuni.2014.04.015.

68. Ip, W.K.E., Hoshi, N., Shouval, D.S., Snapper, S., and Medzhitov, R. (2017). Anti-inflammatory effect of IL-10 mediated by metabolic reprogramming of macrophages. Science *356*, 513–519. https://doi.org/10.1126/science.aal3535.

69. Kühn, R., Löhler, J., Rennick, D., Rajewsky, K., and Müller, W. (1993). Interleukin-10-deficient mice develop chronic enterocolitis. Cell *75*, 263–274. https://doi.org/10.1016/0092-8674(93)80068-P.

70. Denning, T.L., Wang, Y.C., Patel, S.R., Williams, I.R., and Pulendran, B. (2007). Lamina propria macrophages and dendritic cells differentially induce regulatory and interleukin 17-producing T cell responses. Nat. Immunol. *8*, 1086–1094. https://doi.org/10.1038/ni1511.

71. Morhardt, T.L., Hayashi, A., Ochi, T., Quirós, M., Kitamoto, S., Nagao-Kitamoto, H., Kuffa, P., Atarashi, K., Honda, K., Kao, J.Y., et al. (2019). IL-10 produced by macrophages regulates epithelial integrity in the small intestine. Sci. Rep. *9*, 1223. https://doi.org/10.1038/s41598-018-38125-x.

72. Hennessy, E.J., Parker, A.E., and O'Neill, L.A. (2010). Targeting toll-like receptors: emerging therapeutics? Nat. Rev. Drug Discov. *9*, 293–307. https://doi.org/10.1038/nrd3203.

73. Miller, R.S., and Hoskins, L.C. (1981). Mucin degradation in human colon ecosystems. Fecal population densities of mucin-degrading bacteria estimated by a "most probable number" method. Gastroenterology *81*, 759–765.

74. Ottman, N., Davids, M., Suarez-Diez, M., Boeren, S., Schaap, P.J., Martins Dos Santos, V.A.P., Smidt, H., Belzer, C., and de Vos, W.M. (2017). Genome-scale model and omics analysis of metabolic capacities of Akkermansia muciniphila Reveal a preferential mucin-degrading lifestyle. Appl. Environ. Microbiol. *83*. https://doi.org/10.1128/AEM.01014-17.

75. van der Ark, K.C.H., Aalvink, S., Suarez-Diez, M., Schaap, P.J., de Vos, W.M., and Belzer, C. (2018). Model-driven design of a minimal medium for Akkermansia muciniphila confirms mucus adaptation. Microb. Biotechnol. *11*, 476–485. https://doi.org/10.1111/1751-7915.13033.

76. Schrager, J. (1970). The chemical composition and function of gastrointestinal mucus. Gut *11*, 450–456. https://doi.org/10.1136/gut.11.5.450.

77. M'Koma, A.E. (2013). Inflammatory bowel disease: an expanding global health problem. Clin. Med. Insights Gastroenterol. *6*, 33–47. https://doi.org/10.4137/CGast.S12731.

78. Ananthakrishnan, A.N. (2015). Epidemiology and risk factors for IBD. Nat. Rev. Gastroenterol. Hepatol. *12*, 205–217. https://doi.org/10.1038/nrgastro.2015.34.

79. Glassner, K.L., Abraham, B.P., and Quigley, E.M.M. (2020). The microbiome and inflammatory bowel disease. J. Allergy Clin. Immunol. *145*, 16–27. https://doi.org/10.1016/j.jaci.2019.11.003.

80. Zigmond, E., Bernshtein, B., Friedlander, G., Walker, C.R., Yona, S., Kim, K.W., Brenner, O., Krauthgamer, R., Varol, C., Müller, W., et al. (2014). Macrophage-restricted interleukin-10 receptor deficiency, but not IL-10 deficiency, causes severe spontaneous colitis. Immunity *40*, 720–733. https://doi.org/10.1016/j.immuni.2014.03.012.

81. Shouval, D.S., Biswas, A., Goettel, J.A., McCann, K., Conaway, E., Redhu, N.S., Mascanfroni, I.D., Al Adham, Z., Lavoie, S., Ibourk, M., et al. (2014). Interleukin-10 receptor signaling in innate immune cells regulates mucosal immune tolerance and anti-inflammatory macrophage function. Immunity *40*, 706–719. https://doi.org/10.1016/j.immuni.2014.03.011.

82. Marlow, G.J., van Gent, D., and Ferguson, L.R. (2013). Why interleukin-10 supplementation does not work in Crohn's disease patients. World J. Gastroenterol. *19*, 3931–3941. https://doi.org/10.3748/wjg.v19.i25.3931.

83. Yim, J., Cho, S.W., Kim, B., Park, S., Han, Y.H., and Seo, S.W. (2020). Transcriptional profiling of the probiotic Escherichia coli Nissle 1917 Strain under simulated microgravity. Int. J. Mol. Sci. *21*, 2666.

84. Gack, M.U., Shin, Y.C., Joo, C.H., Urano, T., Liang, C., Sun, L., Takeuchi, O., Akira, S., Chen, Z., Inoue, S., et al. (2007). TRIM25 RING-finger E3 ubiquitin ligase is essential for RIG-I-mediated antiviral activity. Nature *446*, 916–920. https://doi.org/10.1038/nature05732.

85. Mirdita, M., Steinegger, M., and Söding, J. (2019). MMseqs2 desktop and local web server app for fast, interactive sequence searches. Bioinformatics *35*, 2856–2858. https://doi.org/10.1093/bioinformatics/bty1057.

86. Tyanova, S., Temu, T., and Cox, J. (2016). The MaxQuant computational platform for mass spectrometry-based shotgun proteomics. Nat. Protoc. *11*, 2301–2319. https://doi.org/10.1038/nprot.2016.136.

87. Tyanova, S., Temu, T., Sinitcyn, P., Carlson, A., Hein, M.Y., Geiger, T., Mann, M., and Cox, J. (2016). The Perseus computational platform for comprehensive analysis of (prote)omics data. Nat. Methods *13*, 731–740. https://doi.org/10.1038/nmeth.3901.

88. Dobin, A., Davis, C.A., Schlesinger, F., Drenkow, J., Zaleski, C., Jha, S., Batut, P., Chaisson, M., and Gingeras, T.R.J.B. (2013). STAR: ultrafast universal RNA-seq aligner. Bioinformatics *29*, 15–21. https://doi.org/10.1093/bioinformatics/bts635.

89. Goldman, M.J., Craft, B., Hastie, M., Repečka, K., McDade, F., Kamath, A., Banerjee, A., Luo, Y., Rogers, D., Brooks, A.N.J.N.b., et al. (2020). Visualizing and interpreting cancer genomics data via the Xena platform. Nat. Biotechnol. *38*, 675–678. https://doi.org/10.1038/s41587-020-0546-8.

90. Howe, E.A., Sinha, R., Schlauch, D., and Quackenbush, J.J.B. (2011). RNA-Seq analysis in MeV. Bioinformatics *27*, 3209–3210. https://doi.org/10.1093/bioinformatics/btr490.

91. Kolde, R., and Kolde, M.R.J.R.p. (2015). Package 'pheatmap'*1*, p. 790.

92. Subramanian, A., Tamayo, P., Mootha, V.K., Mukherjee, S., Ebert, B.L., Gillette, M.A., Paulovich, A., Pomeroy, S.L., Golub, T.R., Lander, E.S., et al. (2005). Gene set enrichment analysis: a knowledge-based approach for interpreting genome-wide expression profiles. Proc. Natl. Acad. Sci. USA *102*, 15545–15550. https://doi.org/10.1073/pnas.0506580102.

93. Kuleshov, M.V., Jones, M.R., Rouillard, A.D., Fernandez, N.F., Duan, Q., Wang, Z., Koplev, S., Jenkins, S.L., Jagodnik, K.M., Lachmann, A., et al. (2016). Enrichr: a comprehensive gene set enrichment analysis web server 2016 update. Nucleic Acids Res. *44*, W90–W97. https://doi.org/10.1093/nar/gkw377.

94. Mallick, H., Rahnavard, A., McIver, L.J., Ma, S., Zhang, Y., Nguyen, L.H., Tickle, T.L., Weingart, G., Ren, B., Schwager, E.H., et al. (2021). Multivariable association discovery in population-scale meta-omics studies. PLoS Comput. Biol. *17*, e1009442. https://doi.org/10.1371/journal.pcbi.1009442.

95. Perez-Riverol, Y., Bai, J., Bandla, C., García-Seisdedos, D., Hewapathirana, S., Kamatchinathan, S., Kundu, D.J., Prakash, A., Frericks-Zipper, A., Eisenacher, M., et al. (2022). The PRIDE database resources in 2022: a hub for mass spectrometry-based proteomics evidences. Nucleic Acids Res. *50*, D543–D552. https://doi.org/10.1093/nar/gkab1038.

96. Derrien, M., Vaughan, E.E., Plugge, C.M., and de Vos, W.M. (2004). Akkermansia muciniphila gen. nov., sp. nov., a human intestinal mucin-degrading bacterium. Int. J. Syst. Evol. Microbiol. *54*, 1469–1476. https://doi.org/10.1099/ijs.0.02873-0.

97. Stams, A.J., Van Dijk, J.B., Dijkema, C., and Plugge, C.M. (1993). Growth of syntrophic propionate-oxidizing bacteria with fumarate in the absence of methanogenic bacteria. Appl. Environ. Microbiol. *59*, 1114–1119. https://doi.org/10.1128/aem.59.4.1114-1119.1993.

98. Ahn, S., Jin, T.E., Chang, D.H., Rhee, M.S., Kim, H.J., Lee, S.J., Park, D.S., and Kim, B.C. (2016). Agathobaculum butyriciproducens gen. nov. sp. nov., a strict anaerobic, butyrate-producing gut bacterium isolated from human faeces and reclassification of Eubacterium desmolans as Agathobaculum desmolans comb. nov. Int. J. Syst. Evol. Microbiol. *66*, 3656–3661. https://doi.org/10.1099/ijsem.0.001195.

99. Murthy, S.N., Cooper, H.S., Shim, H., Shah, R.S., Ibrahim, S.A., and Sedergran, D.J. (1993). Treatment of dextran sulfate sodium-induced murine colitis by intracolonic cyclosporin. Dig. Dis. Sci. *38*, 1722–1734. https://doi.org/10.1007/BF01303184.

100. Sellon, R.K., Tonkonogy, S., Schultz, M., Dieleman, L.A., Grenther, W., Balish, E., Rennick, D.M., and Sartor, R.B. (1998). Resident enteric bacteria are necessary for development of spontaneous colitis and immune system activation in interleukin-10-deficient mice. Infect. Immun. *66*, 5224–5231. https://doi.org/10.1128/IAI.66.11.5224-5231.1998.

101. Li, M.Z., and Elledge, S.J. (2012). SLIC: A method for sequence- and ligation-independent cloning. Methods Mol. Biol. *852*, 51–59. https://doi.org/10.1007/978-1-61779-564-0_5.

102. Teodorowicz, M., Perdijk, O., Verhoek, I., Govers, C., Savelkoul, H.F., Tang, Y., Wichers, H., and Broersen, K. (2017). Optimized Triton X-114 assisted lipopolysaccharide (LPS) removal method reveals the immunomodulatory effect of food proteins. PLoS One *12*, e0173778. https://doi.org/10.1371/journal.pone.0173778.

103. Liu, J.H., Chen, C.Y., Liu, Z.Z., Luo, Z.W., Rao, S.S., Jin, L., Wan, T.F., Yue, T., Tan, Y.J., Yin, H., et al. (2021). Extracellular vesicles from child gut microbiota enter into bone to preserve bone mass and strength. Adv. Sci. (Weinh) *8*, 2004831. https://doi.org/10.1002/advs.202004831.

104. Chuang, L.S., Morrison, J., Hsu, N.Y., Labrias, P.R., Nayar, S., Chen, E., Villaverde, N., Facey, J.A., Boschetti, G., Giri, M., et al. (2019). Zebrafish modeling of intestinal injury, bacterial exposures and medications defines epithelial in vivo responses relevant to human inflammatory bowel disease. Dis. Model. Mech. *12*. https://doi.org/10.1242/dmm.037432.

105. Jiang, Y., Chen, B., Duan, C., Sun, B., Yang, J., and Yang, S. (2015). Multigene editing in the Escherichia coli genome via the CRISPR-Cas9 system. Appl. Environ. Microbiol. *81*, 2506–2514. https://doi.org/10.1128/AEM.04023-14.

STAR★METHODS

KEY RESOURCES TABLE

REAGENT or RESOURCE	SOURCE	IDENTIFIER
Antibodies		
Mouse monoclonal anti-Strep	IBA	Cat# 2-1509-001
Mouse monoclonal anti-FLAG	Cell signaling technology	Cat# 8146; RRID: AB_10950495
Rabbit monoclonal anti-β-Actin	Cell signaling technology	Cat# 12620; RRID: AB_2797972
Rabbit polyclonal anti-phospho-ERK1/2 (T202/Y204)	Cell signaling technology	Cat# 9101; RRID: AB_331646
Rabbit monoclonal anti-ERK1/2	Cell signaling technology	Cat# 4695; RRID: AB_390779
Rabbit monoclonal anti-phospho-p38 MAPK (T180/Y182)	Cell signaling technology	Cat# 4511; RRID: AB_2139682
Rabbit monoclonal anti-p38 MAPK	Cell signaling technology	Cat# 8690; RRID: AB_10999090
Rabbit polyclonal anti-phospho-MSK1 (T581)	Cell signaling technology	Cat# 9595; RRID: AB_2181783
Rabbit monoclonal anti-phospho-NF-κB p65 (S536)	Cell signaling technology	Cat# 3033; RRID: AB_331284
Rabbit monoclonal anti-NF-κB p65	Cell signaling technology	Cat# 8242; RRID: AB_10859369
Rabbit monoclonal anti-phospho-CREB (S133)	Cell signaling technology	Cat# 9198; RRID: AB_2561044
Rabbit monoclonal anti-CREB	Cell signaling technology	Cat# 9197; RRID: AB_331277
Rabbit monoclonal anti-phospho-GSK-3β (S9)	Cell signaling technology	Cat# 5558; RRID: AB_10013750
Rabbit monoclonal anti-GSK-3β	Cell signaling technology	Cat# 12456; RRID: AB_2636978
Rabbit monoclonal anti-phospho-PI3 Kinase (Y458/Y199)	Cell signaling technology	Cat# 17366; RRID: AB_2895293
Rabbit monoclonal anti-PI3 Kinase p55	Cell signaling technology	Cat# 11889; RRID: AB_2797756
Rabbit monoclonal anti-phospho-AKT (S473)	Cell signaling technology	Cat# 4060; RRID: AB_2315049
Rabbit monoclonal anti-AKT (pan)	Cell signaling technology	Cat# 4691; RRID: AB_915783
Horse anti-mouse IgG, HRP-conjugated	Cell signaling technology	Cat# 7076; RRID: AB_330924
Goat anti-rabbit, HRP-conjugated	Cell signaling technology	Cat# 7074; RRID: AB_2099233
Goat polyclonal anti-MSK1	R&D systems	Cat# AF2518; RRID: AB_2301227
Rabbit anti-goat IgG, HRP-conjugated	R&D systems	Cat# HAF017; RRID: AB_562588
Mouse monoclonal anti-MSK2	Santa Cruz Biotechnology	Cat# sc-377151
Rabbit polyclonal anti-MSK2 (T568)	Assay Biotech	Cat# A8149; RRID: AB_10684516
Armenian Hamster Anti-CD3e, FITC-conjugated	BD Biosciences	Cat# 553062; RRID:AB_394595
Rat monoclonal anti-CD19, FITC-conjugated	BD Biosciences	Cat# 553785; RRID: AB_395049
Rat monoclonal anti-CD4, PE-conjugated	BD Biosciences	Cat# 553730; RRID: AB_395014
Rat monoclonal anti-IL10, PE-conjugated	BD Biosciences	Cat# 554467; RRID: AB_395412
Rat monoclonal anti-CD11b, PE-Cy7-conjugated	BD Biosciences	Cat# 552850; RRID: AB_394491
Rat monoclonal anti-F4/80, APC-conjugated	BD Biosciences	Cat# 565853; RRID: AB_2744474
Hamster monoclonal anti-CD11c, APC-Cy7-conjugated	BD Biosciences	Cat# 561241; RRID: AB_10611727
Rat monoclonal anti-CD8, APC-conjugated	BD Biosciences	Cat# 553035; RRID: AB_398527
Rat monoclonal anti-CD206 (MMR), Alexa Fluor 488-conjugated	ThermoFisher	Cat# 53-2061-82; RRID: AB_2784749
Rat monoclonal anti-mouse Mac2	CEDARLANE	Cat# CL8942AP; RRID: AB_10060357
Rabbit polyclonal anti-rat IgG, FITC-conjugated	abcam	Cat# ab6730; RRID: AB_955327
Mouse monoclonal anti-6X His tag antibody	Invitrogen	Cat# MA1-135; RRID: AB_2536841
Rabbit monoclonal anti-His tag	Cell signaling technology	Cat# 12698; RRID: AB_2744546
Rat monoclonal anti-F4/80	Abcam	Cat# ab6640; RRID: AB_1140040
Rabbit polyclonal anti-IgG	Santa Cruz Biotechnology	Cat# sc-66931; RRID: AB_1125055

(*Continued on next page*)

Continued

REAGENT or RESOURCE	SOURCE	IDENTIFIER
Mouse monoclonal anti-hTLR1	Invivogen	Cat# mabg-htlr1; RRID: AB_11124907
Mouse monoclonal anti-mTLR2	Invivogen	Cat# mabg-mtlr2; RRID: AB_11125339
Hamster monoclonal anti-hTLR2	Invivogen	Cat# maba2-htlr2; RRID: AB_11142484
Mouse monoclonal anti-hTLR6	Invivogen	Cat# mabg-htlr6; RRID: AB_11142485
Rabbit polyclonal anti-*Am*TARS	This paper	N/A
Rabbit polyclonal anti-*Am*YARS	This paper	N/A
Rabbit polyclonal anti-*Am*GAPDH	This paper	N/A
Bacterial strains		
A. muciniphila MucT	German Collection of Microorganisms and Cell Cultures GmbH	Cat# DSM 22959
E. Coli: NiCo21(DE3) Competent	NEB	Cat# C2529H
ClearColi® BL21(DE3) Electrocompetent Cells	Lucigen	Cat# 60810
E. coli: Nissle 1917 (*Ec*N)	Yim et al.[83]	N/A
E. coli: Nissle 1917::*Am*TARS (*Ec*N(AmTARS))	This paper	N/A
Chemicals, peptides, and recombinant proteins		
Dextran sulfate sodium salt, colitis grade	MP biomedical	Cat# 160110
Lipopolysaccharides from *E. coli* O111:B4 (LPS)	Sigma	Cat# L2630
Phorbol 12-myristate 13-acetate (PMA)	Sigma	Cat# P8139
Pam3CSK4	Invivogen	Cat# tlrl-pms
Recombinant IL-4	Peprotech	Cat# 200-04
Recombinant IL-13	Peprotech	Cat# 200-13
Recombinant mouse IL-10	BioLegend	Cat# 575806
Encapsome	Encapsula Nano Sciences	Cat# CLD-8910
Clodrosome	Encapsula Nano Sciences	Cat# CLD-8909
SCREEN-WELL® Kinase Inhibitor library	Enzo Lifesciences	Cat# BML-2832
Polyethylenimine	Polybiosciences	Cat# 23966
Triton X-114	Sigma	Cat# X114
3X FLAG peptide	Sigma	Cat# F4799
Porcine gastric mucin (Type III)	Sigma	Cat# M1778
8% Paraformaldehyde in 2X PBS	Biosesang	Cat# PC2184-050-00
Sucrose	Sigma	Cat# S7903; CAS# 57-50-1
Magnesium sulfate heptahydrate	Sigma	Cat# 63138; CAS# 10034-99-8
Potassium chloride	Sigma	Cat# P5405; CAS# 7447-40-7
Sodium chloride	Sigma	Cat# S7653; CAS# 7647-14-5
Calcium chloride dehydrate	Sigma	Cat# C7902; CAS# 10035-04-8
Ethyl 3-aminobenzoate methanesulfonate salt	Sigma	Cat# S5040; CAS# 886-86-2
Sodium citrate	Sigma	Cat# S464; CAS# 6132-04-3
Agarose, Low Melting Point, Analytical Grade	Promega	Cat# V2111
Mounting Medium with DAPI	abcam	Cat# ab104139
Optiprep solution (60% (w/v))	Sigma	Cat# D1556; CAS# 92339-11-2
Critical commercial assays		
BD OptEIA™ Mouse IL-6 ELISA set	BD Biosciences	Cat# 555240; RRID: AB_2869049
BD OptEIA™ Mouse IL-10 ELISA Set	BD Biosciences	Cat# 555252; RRID: AB_2869052
BD OptEIA™ Mouse TNF (Mono/Mono) ELISA Set	BD Biosciences	Cat# 555268; RRID: AB_2869055
BD OptEIA™ Human IL-6 ELISA Set	BD Biosciences	Cat# 555220; RRID: AB_2869045

(*Continued on next page*)

Continued

REAGENT or RESOURCE	SOURCE	IDENTIFIER
BD OptEIA™ Human IL-10 ELISA Set	BD Biosciences	Cat# 555157; RRID: AB_2869031
BD OptEIA™ Human TNF ELISA Set	BD Biosciences	Cat# 555212; RRID: AB_2869042
Experimental models: cell lines		
Human: HEK 293T cells	ATCC	Cat# CRL-11268; RRID: CVCL_1926
Human: THP-1 cells	KCLB	Cat# 40202; RRID: CVCL_0006
Human: HEK Blue-TLR4 cells	Invivogen	Cat# 293-htlr4a; RRID: CVCL_Y393
Experimental models: organisms/strains		
Mouse: C57BL/6J	The Jackson Laboratory	JAX 000664
Mouse: Tlr2 KO (B6.129-Tlr2tm1Kir/J)	The Jackson Laboratory	JAX 004650
Mouse: B6-CD45.1	The Jackson Laboratory	JAX 002014
Zebrafish: AB strain (wild type)	ZIRC	ZDB-GENO-960809-7
Zebrafish: *Tg(NFκB:EGFP)*	Lee et al.[57]	N/A
Oligonucleotides: primers used for bacterial engineering		
Primers targeting the upstream region of *exo/cea*: CTCAGGTTACCCGCATGAAACCAGA CTGAAGC (forward), CGAGCCGATGATTAATTGTCAACGT AAATGATTGCGG (reverse)	This paper	N/A
Primers targeting the downstream region of exo/cea: CTTGTCTGTAAGCGGATGCCATTTACG TTATCCAGACG (forward), CTCGAGTACGCGTCAGGGTTGACAG GGAAAAC (reverse)	This paper	N/A
Primers used to insert the exo/cea-targeting sequence into pTarget: CTGGATAACGTAAATGATTGGTTTTA GAGCTAGAAATAG (forward), CAATCATTTACGTTATCCAGACTAGT ATTATACCTAGGAC (reverse)	This paper	N/A
Recombinant DNA		
pET21a vector	Novagen	Cat# 69740
pET21a-*Am*AARS	This paper	N/A
pET21a-*Am*CARS	This paper	N/A
pET21a-*Am*DARS	This paper	N/A
pET21a-*Am*EARS	This paper	N/A
pET21a-*Am*FARSa	This paper	N/A
pET21a-*Am*FARSb	This paper	N/A
pET21a-*Am*GARS	This paper	N/A
pET21a-*Am*HARS	This paper	N/A
pET21a-*Am*IARS	This paper	N/A
pET21a-*Am*KARS	This paper	N/A
pET21a-*Am*LARS	This paper	N/A
pET21a-*Am*MARS	This paper	N/A
pET21a-*Am*NARS	This paper	N/A
pET21a-*Am*PARS	This paper	N/A
pET21a-*Am*QARS	This paper	N/A
pET21a-*Am*RARS	This paper	N/A
pET21a-*Am*TARS	This paper	N/A
pET21a-*Am*VARS	This paper	N/A

(*Continued on next page*)

Continued

REAGENT or RESOURCE	SOURCE	IDENTIFIER
pET21a-*Am*WARS	This paper	N/A
pET21a-*Am*YARS	This paper	N/A
pET21a-*Am*GAPDH	This paper	N/A
pET21a- ΔU1*Am*TARS	This paper	N/A
pET21a- ΔU2*Am*TARS	This paper	N/A
pET21a- ΔU1ΔU2*Am*TARS	This paper	N/A
pET21a-*Am*TARS_NTD	This paper	N/A
pET21a-*Am*TARS_CD	This paper	N/A
pET21a-*Am*TARS_ΔU2CD	This paper	N/A
pET21a-*Am*TARS_ABD	This paper	N/A
pET21a-*Bf*TARS	This paper	N/A
pET21a-*Ec*TARS	This paper	N/A
pET21a-*Ec*TARS (U1/U2)	This paper	N/A
pET21a-*Rb*TARS	This paper	N/A
pET22b(+) vector	Novagen	Cat# 69744-3
pET22b(+)-*Hs*TARS	This paper	N/A
pIRES-FLAG vector	Gack et al.[84]	N/A
pIRES-NLRX1-FLAG	This paper	N/A
pIRES-CD163-FLAG	This paper	N/A
pIRES-TLR4-FLAG	This paper	N/A
pCMV3-TLR2-FLAG	Sino Biological	Cat# HG10061-CF
pEXPR-IBA105 vector	IBA	Cat# 2-3505-000
pEXPR-IBA105-*Am*TARS	This paper	N/A
pCas	Addgene	Cat# 62225
pTarget	Addgene	Cat# 62226
Software and algorithms		
Prism (v6.0)	N/A	http://www.graphpad.com
CellQuest pro	BD biosciences	N/A
AlphaFold2_advanced	Jumper et al.[43]	https://colab.research.google.com/github/sokrypton/ColabFold/blob/main/beta/AlphaFold2_advanced.ipynb
MMseqs2	Mirdita et al.[85]	https://github.com/soedinglab/MMseqs2
PyMOL (v1.8.6.0)	Schrödinger, LLC	https://pymol.org/2/
MaxQuant (v1.6.10.43 and v2.1.1.0)	Tyanova et al.[86]	https://www.maxquant.org
Perseus (v1.5.8)	Tyanova et al.[87]	https://www.maxquant.org/perseus/
STAR (v2.5.1)	Dobin et al.[88]	N/A
edgeR (v3.12.1)	Goldman et al.[89]	N/A
MeV	Howe et al.[90]	https://mev.tm4.org/
R pheatmap package (v1.0.12)	Kolde et al.[91]	https://cran.r-project.org/web/packages/pheatmap/index.html
GSEA (v4.0.0)	Subramanian et al.[92]	https://www.gsea-msigdb.org/gsea/index.jsp
Enrichr	Kuleshov et al.[93]	https://maayanlab.cloud/Enrichr/
MaAsLin2 (v1.2.0)	Mallick et al.[94]	N/A
Deposited data		
Raw LC-MS/MS data, the results of interactome analysis and proteomic analysis of EV and EV-free supernatant from *A. muciniphila*	This paper	PRIDE Archive: PXD041790
Other		
Ni-NTA Agarose	QIAGEN	Cat# 30230
Strep-Tactin® Sepharose® resin	IBA	Cat# 2-1201-002

(*Continued on next page*)

Continued

REAGENT or RESOURCE	SOURCE	IDENTIFIER
SnakeSkin, Dialysis tubing, 10K MWCO	ThermoFisher	Cat# 68100
Slide-A-Lyzer Dialysis Cassette G2, 10K MWCO	ThermoFisher	Cat# 87730
Bolt 4-12%, Bis-Tris, 1.0 mm, Mini Protein Gels	Invitrogen	Cat# NW04125BOX
iBlot 2 Transfer Stacks, PVDF	Invitrogen	Cat# IB24002
Mem-PER Plus Membrane Protein Extraction Kit	ThermoFisher	Cat# 89842
HEK Blue selection (250X concentrate)	Invivogen	Cat# hb-sel
HEK Blue detection	Invivogen	Cat# hb-det
Protease inhibitor cocktail	GenDEPOT	Cat# P3100
Phosphatase inhibitor cocktail	GenDEPOT	Cat# P3200
Alexa Fluor 568 Protein Labeling Kit	Invitrogen	Cat# A102238

RESOURCE AVAILABILITY

Lead contact

For information and requests about resources and reagents used in this study, please contact the lead contact Myung Hee Kim (mhk8n@kribb.re.kr).

Materials availability

Materials are available from the lead contact upon request.

Data and code availability

- The mass spectrometry proteomics data generated in this study have been deposited to the ProteomeXchange Consortium via the PRIDE[95] database with the dataset identifier PXD041790.
- This paper does not report original code.
- Any additional information required to reanalyze the data reported in this work paper is available from the lead contact upon request.

EXPERIMENTAL MODEL AND SUBJECT DETAILS

Mice

C57BL/6J mice were purchased from Damul Science (Daejeon, Korea). Tlr2-KO (B6.129-Tlr2tm1Kir/J) and B6-CD45.1 (B6.SJL-Ptprca Pepcb/BoyJ) mice were purchased from Jackson Laboratory (Bar Harbor, ME). All mice were maintained under specific pathogen-free conditions on a 12 h light/dark cycle at 22±1°C, and all offspring were genotyped using RT-PCR prior to use in experiments. All experiments using mice were performed according to the guidelines of the Institutional Animal Use and Care Committee of Korea Research Institute of Bioscience and Biotechnology (KRIBB-AEC-20030).

Isolation of primary cells

The large intestine was removed from mice, cut longitudinally into 0.5–1 cm lengths, and washed gently with phosphate-buffered saline (PBS) buffer (137 mM NaCl, 2.7 mM KCl, 10 mM Na_2HPO_4, and 1.8 mM KH_2PO_4). Washed tissues were transferred to 50 ml conical tubes containing 5 ml of RPMI-1640 (Gibco) plus 1 mg ml^{-1} type IV collagenase (Sigma, St. Louis, MO) and incubated in a shaking incubator at 250 rpm for 30 min. After digestion, tissue derivatives were filtered through mesh (100 micron) and centrifuged at 500 × g at 4°C for 5 min, and the cell pellets were re-suspended in PBS. Peritoneal exudate cells (PECs) were collected by delivering 10 ml of cold RPMI 1640 containing 2% (v/v) fetal bovine serum (FBS) (Gibco) into the peritoneal cavity and gently aspirating the fluid. The fluid lavage was centrifuged at 500 × g at 4°C for 3 min and pellets were re-suspended in PBS. PECs were cultured in Dulbecco's Modified Eagle Medium (DMEM; Hyclone) containing 10% (v/v) FBS. To purify macrophages, isolated intestinal and peritoneal cells were stained with CD11b-PE and F4/80-APC antibodies, and $CD11b^+F4/80^+$ double-positive cells were sorted using a FACSAria™ III (BD). BMDMs were isolated from 7–8-week-old mice, and red blood cells were lysed with ACK lysis buffer (Gibco). BMDMs were cultured for 5 days in DMEM containing 10% (v/v) FBS and 50 ng ml^{-1} GM-CSF (R&D systems); the medium was replaced with fresh complete medium every other day. Next, BMDMs were stimulated for 24 h with 10 ng ml^{-1} LPS (Sigma) to induce inflammatory responses, or with 20 ng ml^{-1} IL-4 (Peprotech) and 20 ng ml^{-1} IL-13 (Peprotech) to induce M2 polarization.

HEK293T cell lines

The human kidney epithelial cell line HEK293T (ATCC) was maintained in DMEM containing 10% (v/v) FBS (Gibco) and 1% (v/v) Antibiotic-Antimycotic (Gibco). HEK Blue-TLR4 cells (InvivoGen) were grown in DMEM containing 10% (v/v) FBS, 1% (v/v)

Antibiotic-Antimycotic, 100 μg ml^{-1} Normocin (InvivoGen), and 1X HEK Blue selection (InvivoGen). The cell lines were incubated at 37°C in 5% (v/v) CO_2.

THP-1 cell line

The human leukemia monocyte cell line THP-1 (ATCC) was grown at 37°C/5% (v/v) CO_2 in RPMI 1640 medium (Gibco) containing 10% (v/v) FBS and 1% (v/v) Antibiotic-Antimycotic. THP1 cells were differentiated to adherent macrophage-like phenotype by treatment with 10 ng ml^{-1} Phorbol 12-myristate 13-acetate (PMA, Sigma) for 48 h. Culture medium was replaced with fresh medium daily.

A. muciniphila culture

A. muciniphila Muc^T (=DSM 22959^T) was cultivated anaerobically at 37°C in basal medium[96] supplemented with 16 g l^{-1} soy-peptone, 25 mM glucose, and 0.05% porcine gastric mucin (Type III, Sigma). The trace element and vitamin solutions were as described previously.[97] All compounds were autoclaved, except the vitamins, which were filter-sterilized. All procedures for media preparation were performed under anaerobic conditions according to previously established methods.[98]

Zebrafish husbandry

Adult zebrafish (*Danio rerio*) AB (wild type, WT) strain and *Tg(NFκB:EGFP)* were maintained at 28.5°C under standard conditions. The *Tg(NFκB:EGFP)* line was used as a NF-κB activity reporter to measure intestinal NF-κB activity.[57] Fish were fed daily with a dry food and maintained under a light/dark schedule of 14 h and 10 h dark. Zebrafish husbandry and animal care were performed in accordance with guidelines from the Korea Research Institute of Bioscience and Biotechnology (KRIBB), and all experiments were approved by KRIBB-AEC-22179.

METHOD DETAILS

Induction of DSS-induced colitis and measurement of disease activity

Mice were administered 2% DSS (molecular weight 36–50 kDa; MP Biomedicals, Santa Ana, CA) via their drinking water for 10 days. Proteins, including *Am*TARS, *Am*TARS deletion mutants, and mouse IL-10 (BioLegend), were i.p.-injected every other day. The amounts of protein given to mice are described in the figure legends. To deplete macrophages from mice, 200 μl of Clodrosome (clodronate encapsulated liposomes; Encapsula Nano Sciences) or Encapsome (control liposomes) was i.p.-injected 4 days before administration of DSS and on Days 0, 2, 4, and 6 during DSS administration. Treatment with engineered *Ec*N(AmTARS) or *Ec*N during DSS treatment was performed by oral gavage (daily) with a 100 μl suspension (PBS containing 25% glycerol) containing 10^7 CFU bacteria. Daily clinical assessment of colitis symptoms was carried out by measuring body weight, analyzing stool consistency, and checking for rectal bleeding, which were scored as follows: body weight loss (0, none; 1, 1–5%; 2, 6–10%; 3, 11–15%; 4, >15%), stool consistency (0, well-formed pellets; 2, loose stools; 4, diarrhea), and fecal blood (0, negative hemoccult test; 1, positive hemoccult test; 2, blood visibly present in the stool; 3, blood visibly present and blood clotting on the anus; 4, gross bleeding), as previously described.[99]

H&E and immunofluorescence staining

Colon tissues were fixed overnight at room temperature (RT) fixed in 10% (v/v) formaldehyde, washed for over 6 h with tap water, and embedded using a Tissue Embedding Center module (Tissue-Tek, Sakura Finetek Co., Japan). Tissue sections (7 μm thick) were deparaffinized in xylene and rehydrated in ethanol according to a standard protocol. For histological analysis, tissue sections (7 μm thick) were stained with H&E (Sigma) and imaged under an optical microscope (BX51, Olympus Corp, Tokyo, Japan). The histological scores were determined as described previously.[100] For immunofluorescence staining, the slides were incubated for 15 min at heat with antigen retrieval buffer (0.1 M sodium citrate pH 6.0 and 0.05% Tween-20) and then blocked for 1 h at RT in PBS containing 3% bovine serum albumin. Slices were stained with an anti-mouse Mac2 (CEDARLANE) primary antibody, followed by FITC-conjugated anti-rat IgG (abcam) and anti-6X His tag antibody (Invitrogen) for 2 h at RT, respectively. After washing three times with PBS containing 0.1% Tween-20, slides were mounted in mounting medium containing DAPI (abcam). Images were acquired under a Nikon laser scanning confocal microscope (C2plus) and analyzed using NIS-Elements software.

Flow cytometry

Primary cells were stained with individual fluorescent probe-conjugated antibodies for 30 min at 4°C in FACS buffer (PBS containing 2% (v/v) FBS and 0.05% NaN_3). After washing twice with FACS buffer, stained cells were analyzed using a FACSCalibur®, and data were analyzed using CellQuest software (BD). The following antibodies were used for flow cytometry: FITC-CD3 (553062), FITC-CD19 (553785), PE-CD4 (553730), PE-IL-10 (554467), Cy5.5-CD11b (552850), APC-F4/80 (565853), APC-CD11c (561241), APC-CD8 (553035), and FITC-CD206 (53-2061-82), all from BD Biosciences (San Diego, CA).

Gene cloning

Genes encoding *Akkermansia muciniphila* (*Am*) alanyl-tRNA synthetase (AARS), cysteinyl-tRNA synthetase (CARS), aspartyl-tRNA synthetase (DARS), glutamyl-tRNA synthetase (EARS), phenylalanyl-tRNA synthetase alpha subunit (FARSa), phenylalanyl-tRNA synthetase beta subunit (FARSb), glycyl-tRNA synthetase (GARS), histidyl-tRNA synthetase (HARS), isoleucyl-tRNA synthetase

(IARS), lysyl-tRNA synthetase (KARS), leucyl-tRNA synthetase (LARS), methionyl-tRNA synthetase (MARS), asparaginyl-tRNA synthetase (NARS), prolyl-tRNA synthetase (PARS), glutaminyl-tRNA synthetase (QARS), arginyl-tRNA synthetase (RARS), threonyl-tRNA synthetase (TARS), valyl-tRNA synthetase (VARS), tryptophanyl-tRNA synthetase (WARS), tyrosyl-tRNA synthetase (YARS), and glyceraldehyde 3-phosphate dehydrogenase (GAPDH) were PCR -amplified using *A. muciniphila* Muc^T genomic DNA as a template and then cloned into a pET21a vector encoding a C-terminal hexa-His tag. *Am*TARS deletion mutants (ΔU1*Am*TARS, residues 99–113 deleted; ΔU2*Am*TARS, residues 290–312 deleted; and ΔU1ΔU2*Am*TARS, residues 99–113 and 290–312 double deleted) were cloned into the pET21a vector using the sequence- and ligation-independent cloning (SLIC) method.[101] TARS genes were amplified from genomic DNA isolated from *Bacteroides fragilis*, *Escherichia coli*, and *Ruminococcus bromii*, and then cloned into pET21a. The *E. coli* TARS gene, with the *Am*TARS U1 and U2 regions [*Ec*TARS (U1/U2)] inserted between Gly152 and Glu153, and between Glu323 and Asn324, respectively, was synthesized (Macrogen, South Korea) and cloned into the pET21a vector. All human genes were amplified from HEK 293T cDNA. Human TARS1 was cloned into the pET22b (+) vector, and the human NLRX1, CD163, and TLR4 genes were cloned into the pIRES-FLAG vector, as described previously.[84] For *in vitro* pull-down assay, *Am*TARS domains including N-terminal domain (NTD, residues 1–184), catalytic domain (CD, residues 184–523), ΔU2 catalytic domain (ΔU2CD, deleted the residues 290–312 in CD) and anticodon-binding domain (ABD, residues 524–630) were sub-cloned into the pET21a vector. C-terminal Flag® tagged-human TLR2 was purchased from Sino Biological. For immunoprecipitation analysis, *Am*TARS was sub-cloned into the pEXPR-IBA105 vector (IBA).

Immunoblotting

To determine *Am*TARS-mediated signaling via TLR2, BMDM and differentiated-THP1 cells were treated with 0.5 μM *Am*TARS for 5 min to 3 h. To compare TLR2-mediated signaling by *Am*TARS and Pam3CSK4 (InvivoGen), BMDMs derived from WT and TLR2-KO mice were incubated with 0.5 μM *Am*TARS or 0.5 μM Pam3CSK4 for 30 min. For antibody blocking experiments, BMDMs were pre-treated with TLR antibody (1 μg ml^{-1}, InvivoGen) for 1 h to block TLR2, and then signaling was analyzed following treatment with 0.5 μM *Am*TARS or 0.5 μM Pam3CSK4 at 37°C for 30 min. To evaluate the TLR2 heterodimer preference targeted by *Am*TARS, differentiated-THP1 cells were pre-treated with 1 μg of antibodies (human IgG, anti-hTLR1, anti-hTLR2, and anti-hTLR6) for 1 h and then exposed to 0.5 μM *Am*TARS at 37°C for 30 min. Treated cells were lysed by lysis buffer (50 mM Tris-HCl, pH 7.5, 100 mM NaCl, 1% (v/v) NP-40, 1 mM EDTA, 0.25% (w/v) sodium-deoxycholate, protease inhibitor cocktail (GenDEPOT), and phosphatase inhibitor cocktail (GenDEPOT)), and extracted samples were analyzed by immunoblot. *A muciniphila* culture samples were centrifuged at 5,000 × g for 30 min, and the cells were re-suspended with 1X PBS buffer. Cells were then lysed by sonication (Vibra cell, SONICS). *Am*TARS and *Am*YARS proteins from the lysates and supernatant were analyzed by immunoblotting.

Protein expression and purification

His-tagged ARSs and GAPDH from *A. muciniphila*; TARSs from *B. fragilis*, *E. coli*, *R. bromii*; and human; and *Ec*TARS (U1/U2) were overexpressed in *E. coli* Clear coli BL21 (DE3) cells (Lucigen) by induction with 0.5 mM IPTG at 18°C for 30 h. Plasmids encoding His-tagged *Am*TARS domains were expressed in *E. coli* NiCo21 (DE3) cells (NEB) by induction with 0.5 mM IPTG at 18°C for 18 h. The cells were re-suspended with lysis buffer containing 50 mM Tris-HCl, pH 8.0, 300 mM NaCl, and 10 mM imidazole, pH 8.0; lysed by sonication; and centrifuged at 16,000 × g at 4°C for 1 h. Recombinant proteins purified using Ni-NTA affinity chromatography were eluted by 50 mM Tris-HCl, pH 8.0, 150 mM NaCl and 150 mM imidazole, pH 8.0. The eluted proteins were dialyzed against PBS buffer and purified further using TX-114 detergent to remove LPS as described previously,[102] with some modifications. Briefly, proteins were mixed with 10% (v/v) TX-114 to generate a 2% mixture, incubated at 4°C for 30 min with agitation, and then incubated at 37°C for 10 min. To separate the TX-114 from the mixture, centrifugation was performed at 20,000 × g at 25°C for 3 min. This procedure repeated twice or three times and residual LPS in the proteins was detected by a SEAP reporter assay system using HEK Blue-TLR4 cells. Purified *Am*TARS was labeled with Alexa 568 dye using an Alexa Fluor™ 568 Protein Labeling Kit (Invitrogen). HEK293T cells grown in 150 mm culture dishes were transfected with the TLR2-FLAG construct using PEI. After 24 h, harvested cells were lysed using lysis buffer (50 mM Tris-HCl, pH 7.5, 100 mM NaCl, 1% (v/v) NP-40, 1 mM EDTA, 0.25% (w/v) sodium-deoxycholate, protease inhibitor cocktail, and phosphatase inhibitor cocktail) and clarified by centrifugation at 16,000 × g at 4°C for 1 h. Cell lysates were loaded onto anti-FLAG M2 affinity gel (Sigma) for gravity elution and washed by TBS buffer (50 mM Tris-HCl, pH 7.4, and 137 mM NaCl) with 1% (v/v) NP-40. Bound proteins were eluted with TBS buffer containing 150 μg ml^{-1} of 3X FLAG peptide (Sigma). The purity of the proteins was evaluated by SDS-PAGE followed by Coomassie Brilliant Blue staining (Figure S7H).

Interactome analysis

Differentiated-THP1 cells were lysed and fractionated into membrane and cytosolic proteins using a membrane protein extraction kit (ThermoFisher). The membrane and cytosolic proteins (150 μg each) were incubated at 4°C overnight with *Am*TARS-His (15 μg) with agitation. Ni-NTA resin (QIAGEN) was added to the mixture and incubated at 4°C for 30 min with agitation. Ni-NTA resin was added to the mixture and incubated at 4°C for 30 min with agitation. The resin was washed thoroughly five times with wash buffer (50 mM Tris-HCl, pH 8.0, 300 mM NaCl, and 30 mM imidazole), re-suspended in 1X protein sample buffer, and boiled for 10 min. The samples were analyzed by SDS-PAGE. The protein bands were cut from the gel and destained with 50 mM ammonium bicarbonate/50% acetonitrile (ACN). The proteins present in the gel strips were reduced with dithiothreitol (DTT) and alkylated with iodoacetamide. In-gel digestion was carried out overnight at 37°C using trypsin (Promega), and the resulting peptides were extracted and vacuum dried. The peptides were re-suspended in 0.1% formic acid/2% ACN solution and injected into a LC/MS/MS system. Peptides were separated and

analyzed using an Easy-nanoLC1000 and LTQ-Orbitrap elite (ThermoFisher). The trap column was an Acclaim PepMap 100 (ThermoFisher, 75 μm × 2 cm, C18, 3 μm, 100 Å) column and the analytical column was a PepMap RSLC C18 (ThermoFisher, 2 μm, 100 Å, 75 μm × 50 cm) column. The column temperature was set to 50°C. The mobile phases were 100% water/0.1% formic acid (buffer A) and 100% ACN/0.1% formic acid (buffer B). The column gradient was developed using a linear run from 2% B to 32% B in 120 min at a flow rate of 300 nl min^{-1}. The survey scan settings were as follows: Resolution = 60,000, Max IT = 200 ms, AGC Target = 1E6, mass range ~350–2000 Th. The data dependent analysis (DDA) MS/MS scan settings were as follows: Analyzer = orbitrap; Fragmentation = HCD Top 15 double play; Resolution= 15,000; max IT = 100 ms; AGC target = 5E4; Threshold, 200,000; normalized collision energy = 27%; isolation width = 2.0; dynamic exclusion parameter repeat count 1; repeat duration time for 10 s; exclusion list size = 500; exclusion duration time = 60 sec. LC/MS/MS data were analyzed with MaxQuant92 v1.6.10.43 and Perseus93 v1.5.8. MaxQuant parameters were as follows: database = uniprot homo sapiens, enzyme = trypsin/P, variable modification = Oxidation (M), Acetyl (protein N-term), fixed modification = carbamidomethyl (C), LFQ and match between runs. Protein groups were selected for analysis when 'razor+unique peptide >=2' at Perseus and their LFQ intensity are compared.

Pull-down assay

A cloned Strep-AmTARS gene, along with FLAG-tagged TLR2, NLRX1, CD163 and TLR4 genes, was co-transfected into HEK 293T cells using PEI. Cells were dissolved in lysis buffer containing 50 mM Tris-HCl, pH 7.5, 100 mM NaCl, 1% (v/v) NP-40, 1 mM EDTA, 0.25% (w/v) sodium-deoxycholate, protease inhibitor cocktail, and phosphatase inhibitor cocktail, and lysates were centrifuged at 16,000 × g for 20 min. Extracted proteins were separated by SDS-PAGE. To precipitate Strep-tagged proteins, cells were lysed in lysis buffer, and Strep-Tactin beads (IBA) were added at 4°C for 1 h (with agitation). The beads were washed with lysis buffer and eluted by boiling in 1X protein sample buffer (LPS solution). The precipitated samples were analyzed by SDS-PAGE.

In vitro binding assay

The purified protein mixtures containing TLR2-FLAG with His-tagged *Am*TARS including full-length, NTD, CD, ΔU2 CD, and ABD at a 2:1 ratio were incubated at 4°C for 5 h with agitation. To analyze the U1/U2-mediated interaction with TLR2, purified TLR2-FLAG proteins were mixed with His-tagged *Am*TARS, *Ec*TARS, and *Ec*TARS(U1/U2) at a ratio of 2:1 and then incubated at 4°C for 5 h with agitation. The mixture was loaded onto Ni-NTA resin at 4°C for 30 min, washed ten times with ice-cold wash buffer (50 mM Tris-HCl, pH 7.5, 300 mM NaCl, and 40 mM imidazole), and eluted 1X protein sample buffer (LPS solution). The eluted samples were separated by SDS-PAGE and stained with Coomassie Brilliant Blue.

Enzyme-linked immunosorbent assay (ELISA)

To detect inflammatory cytokines, BMDM cells were stimulated for 24 h with Pam3CSK4 or proteins (i.e., *Am*ARSs, microbiota-derived TARSs, *Ec*TARS (U1/U2), and AmTARS + LPS), after which BMDM supernatants were collected. For the inhibitor studies, BMDMs were pre-treated for 1 h with inhibitors (i.e., PD98,059 (ERK inhibitor, 10 μM), SB203580 (p38 inhibitor, 10 μM), SB747651A (MSK inhibitor, 1 μM), 666-15 (CREB inhibitor, 10 μM), Wortmannin (PI3K inhibitor, 10 μM), and AKT1/2 (AKT inhibitor, 10 μM)) and then incubated with *Am*TARS for 24 h. Differentiated-THP1 cells were treated for 24 h with *Am*TARS under normal and LPS-induced inflammatory conditions. Macrophages derived from PECs and the intestine were treated for 24 h with *Am*TARS. To obtain mice serum, blood was collected from the intraorbital vein and incubated for 4 h at RT. The collected blood was centrifuged at 1,500 × g for 30 min, and the upper serum layer was collected. Cytokine concentrations in cell supernatants and mouse serum were measured by ELISA according to the manufacturer's instructions; mouse IL-6 (555240), mouse IL-10 (555252), mouse TNF (555268), human IL-6 (555220), human IL-10 (555157), and human TNF (555212) (all BD Biosciences).

Isolation of *A. muciniphila* EV

To analyze proteins secreted by *A. muciniphila*, cells were cultured for 24 h in a volume of 1 L; each sample was grown to a density of 2.68, 3.89, and 4.3 × 10^9 cells ml^{-1}. The supernatants were collected from cells cultured in bottles. At first, cells were spun down from the supernatant at 5,000 × g for 15 min at 4°C. The supernatant was collected and spun at 10,000 × g and then 20,000 × g for 15 min at 4°C. The supernatant collected after spinning at 20,000 × g was concentrated 40-fold using a 100K cut-off Amicon centrifugal filter (Merck Millipore). The concentrates were centrifuged at 200,000 for 2 h at 4°C. To isolate EVs from the concentrates, ultra-filtration was performed using Optiprep density gradient ultra-centrifugation.[32,103] The Optiprep solution (60% w/v iodixanol; Sigma Aldrich) formed layers with concentrations from 50% to 10%; the 50% mixture included the concentrates. Briefly, 3 ml of 50%, 3 ml of 40%, 3 ml of 20%, 3 ml of 10% Optiprep, and 1 ml of PBS were layered sequentially and centrifuged at 100,000 × g for 18 h at 4°C in a Himac CP100WX ultra-centrifuge (P40ST-2561).

LC-MS/MS analysis of soluble fractions and EVs from *A. muciniphila*

Samples were digested using Strap micro (PROTIFI) in accordance with the manufacturer's protocol (v4.7). This protocol includes the use of tris (2-carboxyethyl) phosphine (TCEP) and methyl methanethiosulfonate (MMTS) for reduction and alkylation, respectively. Briefly, 1 μg of trypsin/lysC (pierce, part no. A40009) was added to each sample and then incubated overnight at 37°C. Eluted samples were desalted with a home-made stage tip (C18) and dried in a speed-vac. The peptides were re-suspended in 2% acetonitrile/0.1% formic acid solution and then injected into an RSLCnano u3000/Orbitrap Exploris 240 (ThermoFisher) system. The trap column was an Acclaim PepMap 100 (75 μm × 2 cm, C18), and the analytical column was a BEH C18 (75 μm × 25 cm, 1.7 μm, 130Å). The temperature

of both columns was set to 50°C. The mobile phases were 0.1% formic acid in water (buffer A) and 0.1% formic acid in acetonitrile (buffer B). The following gradient was used at a flow rate of 300 nl/min: 2–20% B in 100 min; 20–32% B in 20 min. The survey scan settings are as follows: Resolution = 120,000; Max IT = 50 ms; AGC 300%; mass range 375–1200 Th. The selected precursor was fragmented by HCD and analyzed by orbitrap. Other parameters for the MS/MS scans were as follows: Top15 double play, Resolution = 30,000; max IT = 200 ms; AGC standard; Threshold = 1E5; normalized collision energy = 30%; isolation width = 2; dynamic exclusion parameter exclude after n times = 1; exclusion duration time = 20 s; mass tolerance low/high = 10 ppm. Raw data from LCMSMS were analyzed with MaxQuant v2.1.0.0 and Perseus v1.5.8. MaxQuant parameters were as follows: database = uniprot akkermansia muciniphila; enzyme = trypsin/P; variable modification = Oxidation(M), Acetyl(protein N-term); fixed modification = methylthio (C); LFQ and match between runs = selected. After the proteingroups.txt file was read by Perseus, protein groups were filtered using the 'razor+-unique peptide >=2' criterion. The relative abundance of *Am*TARS and *Am*Omats (outer membrane autotransporter barrel domain proteins) was calculated as the intensity ratio of each protein to total protein in each sample.

DSS-induced zebrafish colitis model

To induce intestinal inflammation in zebrafish, the repeated DSS-injury protocol from Chuang et al.[104] was adopted and modified. Briefly, embryos were generated by outcrossing *Tg(NFκB:EGFP)* with the AB line, followed by maintenance in E3 egg water (5 mM NaCl, 0.17 mM KCl, 0.33 mM $CaCl_2$, 0.33 mM $MgSO_4$). Normally developed embryos showing NF-κB-dependent EGFP expression were sorted at 2 days post fertilization (dpf) using an SZX16 microscope (Olympus). For yolk sac injection, 3 dpf larvae were anesthetized with ethyl 3-aminobenzoate methanesulfonate salt and embedded in 1% low-melting-point agarose (LMA). After solidification of LMA, 2 nl of 1× PBS or AmTARS (0.5 μg/μl) was injected into the yolk sac using a PV830 micro-injector (World Precision Instruments). After injection, larvae were rinsed three times in fresh E3 egg water and treated with 0.5% DSS for 24 h. The next day, larvae were washed/recovered for 24 h in fresh E3 egg water, and re-treated with 0.5% DSS for 24 h to amplify intestinal inflammation. Finally, larvae were fixed overnight at 4°C in 4% PFA solution (4% paraformaldehyde (PFA), 4% sucrose, 0.15 mM $CaCl_2$, 1× PBS), and the intestinal NF-kB activity of 6 dpf larvae was imaged under a high-resolution confocal microscope (see below for details). All animal experiments were repeated at least twice with a minimum of ten zebrafish larvae per group, and were performed at 28.5°C.

Confocal microscopy analysis of intestinal NF-κB activity

Fixed larvae were washed briefly with 1× PBST (1× PBS with 0.1% Tween 20) and embedded in 1% LMA on glass-bottomed imaging dishes. The mid-distal intestinal region that spans the region 250 μm from the anus was imaged using a FV1000 confocal laser scanning microscope (Olympus). Confocal z-projections were made by stacking between nine and ten sections (each 5 μm thick). The relative intensity of NF-kB-dependent EGFP signals in Z-projected images was measured by Image J and the ROI manager. The NF-kB activity of each group was displayed as a percentage relative to the mean fluorescence intensity of PBS-injected WT intestines.

Antibody production

Rabbit polyclonal antibodies specific for *Am*TARS, *Am*YARS, and *Am*GAPDH were produced by Abclon Inc. (Seoul, Korea). Rabbits were immunized with four intraperitoneal injections of 200 μg protein antigen (0, 4, 6, and 8 weeks) in complete Freund's adjuvant (Sigma). Antibodies were purified from serum by IgG purification.

Amino-acylation assay

Threonine-dependent amino-acylation assays were carried out with purified *Am*TARS, ΔU1*Am*TARS, ΔU2*Am*TARS, ΔU1ΔU2*Am*TARS, and *Am*YARS. Assays were performed in reaction buffer (50 mM Tris-HCl, pH 7.5, 10 mM $MgCl_2$, 100 mM NaCl, and 100 mM KCl) containing 1 mM DTT, 250 μM ATP, 2.5 mM L-threonine, 1 U ml^{-1} inorganic pyrophosphatase, and 2 μM of the proteins at 37°C for 30 min, and free inorganic phosphate was detected using malachite green phosphate assay kit (BioAssay Systems) at 620 nm.

Construction of the engineered *Ec*N strain

The engineered *Ec*N strain, which chromosomally expresses C-terminally His-tagged *Am*TARS, was constructed using the lambda red-mediated CRISPR-Cas9 system as previously described.[105] The *exo/cea* intergenic region of the *Ec*N chromosome comprises convergent ORFs; this characteristic has been exploited by other studies to enable insertion of exogeneous sequences while minimizing the effects on expression of neighboring genes.[60,61] The 20 nt sequence of the *exo/cea* intergenic region was cloned into the pTarget vector. His-tagged *Am*TARS and the *lac* promoter were assembled with 500 bp arms homologous to each side of the *exo/cea* intergenic region and then used as the repair template DNA. *Ec*N harboring pCas was transformed with 100 ng of pTarget and the repair template DNA. The resulting engineered *Ec*N was selected and confirmed by PCR encompassing the *exo/cea* intergenic region on the chromosome. To validate expression of His-tagged *Am*TARS by engineered *Ec*N [EcN(*Am*TARS)], the strain was incubated (with shaking) in LB at 37°C. The cells were then spun down from the culture at 10,000 × g for 15 min at 4°C. The supernatant was filtered through a 0.45 μm-pore Minisart syringe filter (Sartorius) and concentrated 40-fold using a 30K cut-off Amicon centrifugal filter (Merck Millipore). The cell lysate and culture supernatant were analyzed by immunoblotting. For comparison, cell lysates equivalent

to the same amount (15 μg) of total protein from EcN(*Am*TARS) or *A. muciniphila* were loaded, and the same volume (40 μl) of concentrated or original culture supernatants from *Ec*N(AmTARS) or *A. muciniphila*, respectively, was loaded.

Adoptive cell transfer

For adoptive transfer, peritoneal cavity cells were isolated from B6-CD45.2 mice and used as donor cells. The isolated cells (5×10^6 per mouse) were transferred intraperitoneally to B6-CD45.1 mice irradiated with a 6 Gy dose (recipients). The mice were then administered *Am*TARS (0.2 mg kg^{-1}) or PBS every other day for 10 days. The number of CD45.2-APC and F4/80-PE-positive cells in the peritoneal cavity and colon was measured by flow cytometry at days 5 and 10 after cell transfer, respectively.

QUANTIFICATION AND STATISTICAL ANALYSIS

Structure modeling of *Am*TARS

A structural model of monomeric *Am*TARS was generated using AlphaFold2_advanced,[43] which is available at https://colab.research.google.com/github/sokrypton /ColabFold/blob/main/beta/ AlphaFold2_advanced.ipynb. The amino acid sequence of *Am*TARS was aligned with multiple sequences produced by MMseqs2.[85] The top five model structures were obtained from the highest pLDDT-scoring model. The structure model of *Am*TARS with the best pLDDT score, 92.53, was selected. All molecular graphics were generated using PyMOL version 1.8.6.0 (Schrödinger, LLC).

RNA sequencing

The PureLink RNA mini kit (ThermoFisher) was used to purify RNAs from BMDMs treated with 0.5 μM *Am*TARS or 10 ng ml^{-1} Pam3CSK4 for 1 or 3 h. An mRNA sequencing library was prepared using the TruSeq RNA Sample Prep Kit (Illumina, San Diego, CA, USA) and sequencing was performed using the Illumina HiSeq2000 platform to generate 100 bp paired-end reads. The reference human genome was obtained from the NCBI genome (https://www.ncbi.nlm.nih.gov/genome/) and genome indexing was performed using the STAR alignment tool (v2.5.1).[88] The sequenced reads were mapped to the human genome (mm10) STAR and gene expression levels were quantified with count module in the STAR aligner. The edgeR (v3.12.1)[89] package was used to select differentially expressed genes from the RNA-seq count data between conditions (-fold change > 1.5, FDR < 0.05). The TMM (the trimmed mean of M-values normalization) normalized CPM (counts per million) value of each gene was added to 1 and $\log_2$-transformed for further analysis. A heatmap was generated using MeV[90] and R (v3.5.0, https://www.r-project.org/) in pheatmap package (v1.0.12, https://cran.r-project.org/web/packages/pheatmap/index.html).

Gene set enrichment analysis (GSEA)

The GSEA software[92] on the Broad Institute website (v4.0.0, https://www.gsea-msigdb.org/gsea/index.jsp) was used for GSEA of RNA-seq data. The expression dataset was analyzed against hallmark, KEGG pathway, and GO gene sets (H, C2, and C5.gmt files from MSigDB v7.0). The statistical significance (nominal p value) of the enrichment score (ES) was calculated by running 1000 gene set permutations. The normalized enrichment score (NES) was used to account for the size of the gene set. Enriched transcription factors (TRANSFAC and JASPAR PWMs) were identified using Enrichr.[93]

Statistical analysis of bacterial tRNA synthetases in iHMP datasets

A public dataset, IBDMDB[36] within iHMP, was used for analyzing the abundance of bacterial tRNA synthetases in disease conditions. iHMP is a longitudinal cohort comprising 132 participants with three clinical diagnoses: non-IBD n = 27; CD (Crohn's disease) n = 67; or UC (Ulcerative colitis) n = 38. IBDMDB provides processed taxonomic and functional profiles from metagenomic (https://ibdmdb.org/tunnel/public/HMP2/WGS/1818/ products) and metatranscriptomic analysis (https://ibdmdb.org/tunnel/public/HMP2/MTX/1750/products). Linear model fitting, using the Microbiome Multivariable Association with Linear Models (MaAsLin2) package (v1.2.0),[94] was used to determine associations between bacterial features and IBD conditions while adjusting for confounding variables. Prior to model fitting, features with low prevalence (cut-off 10%) were removed from the table. Diagnosis, antibiotic, and dysbiosis state were used as categorical or binary variables and age was used as a continuous variable. To adjust effects from repeated measurements over time for the same participants, subjects were coded as a random variable. Of the 1638 metagenome samples from 132 participants, 46 samples were filtered for low sequencing reads (lower than 1 million reads) and of the 835 metatranscriptomic samples, 126 samples were removed for low quality reads or unknown dysbiosis state at the sampling date. Statistical significance was calculated using Wald's test and corrected by the Benjamini-Hochberg method (q-value). Heatmap was used for visualizing abundances of the features by pheatmap package (v1.0.12).[91]

Statistical analyses

Results are presented as the mean ± SEM. Statistical analyses were performed using Prism v.6.0, and p-values were calculated using a two-tailed Student's t-test. The data were considered statistically significant when p-values were <0.05.